Agrobacteria deploy two classes of His-Me finger superfamily nuclease effectors exerting different antibacterial capacities against specific bacterial competitors

Mary Nia M. Santos[acdf], Katherine L. Pintor[a1], Pei-Yu Hsieh[b2], Yee-Wai Cheung[a], Li-Kang Sung[acd], Yu-Ling Shih[b] and Erh-Min Lai[ace*]

[a] Institute of Plant and Microbial Biology, Academia Sinica, Taipei 115201 Taiwan
[b] Institute of Biological Chemistry, Academia Sinica, Taipei 115201 Taiwan
[c] Molecular and Biological Agricultural Sciences Program, Taiwan International Graduate Program, National Chung-Hsing University and Academia Sinica, Taipei, Taiwan
[d] Graduate Institute of Biotechnology, National Chung-Hsing University, Taichung, Taiwan
[e] Biotechnology Center, National Chung-Hsing University, Taichung, Taiwan
[f] Aquaculture Research and Development Division, Department of Agriculture - National Fisheries Research and Development Institute (DA-NFRDI), Manila, Philippines

Running title: His-Me finger T6SS nuclease toxins

*Corresponding author
Erh-Min Lai: emlai@gate.sinica.edu.tw
Institute of Plant and Microbial Biology, Academia Sinica
128 Sec. 2, Academia Road, Nankang, Taipei, Taiwan 115201

Current address:
[1]Department of Ecophysiology, Max Planck Institute for Terrestrial Microbiology, Karl-von-Frisch-Str. 10, 35043 Marburg, Germany
[2]Department of Pharmacology, University of Cambridge, United Kingdom

ORCID
MNMS https://orcid.org/0000-0001-6544-0339
KLP https://orcid.org/0000-0001-9137-4726
PYH https://orcid.org/0000-0002-7263-1691
YWC https://orcid.org/0000-0002-1421-4419
LKS https://orcid.org/0000-0002-7078-8003
YLS https://orcid.org/0000-0002-8232-2569
EML https://orcid.org/0000-0003-3630-8683

ABSTRACT

Type VI secretion system (T6SS) assembles into a contractile nanomachine to inject effectors across bacterial membranes for secretion. *Agrobacterium tumefaciens* species complex is a group of soil inhabitants and phytopathogens that deploys T6SS as an antibacterial weapon against bacterial competitors at both inter-species and intra-species levels. *A. tumefaciens* strain 1D1609 genome encodes one main T6SS gene cluster and four *vrgG* genes (i.e. *vgrGa-d*), each encoding a spike protein as an effector carrier. Previous study reported that *vgrGa*-associated gene 2, named as *v2a,* encodes a His-Me finger nuclease toxin (also named as HNH/ ENDO VII nuclease) contributing to DNase-mediated antibacterial activity. However, the functions and roles of other putative effectors remain unknown. In this study, we identified *vgrGc*-associated gene 2 (*v2c*) that encodes another His-Me finger nuclease but with distinct SHH motif differed from AHH motif of V2a. We demonstrated that the ectopic expression of V2c caused growth inhibition, plasmid DNA degradation, and cell elongation in *Escherichia coli*. The cognate immunity protein, V3c, neutralizes the DNase activity and rescues phenotypes of the growth inhibition and cell elongation. Ectopic expression of V2c DNase-inactive variants retains the cell elongation phenotype while V2a induced cell elongation in a DNase-mediated manner. We also showed that the amino acids of conserved SHH and HNH motifs are responsible for the V2c DNase activity *in vivo* and *in vitro*. Notably, V2c also mediated the DNA degradation and cell elongation of target cell in the context of interbacterial competition. Importantly, V2a and V2c exhibit different capacities against different bacterial species and function synergistically to exert stronger antibacterial activity against the soft rot phytopathogen, *Dickeya dadantii*.

INTRODUCTION

The type VI secretion system (T6SS) is a nanomachine used by many Gram-negative bacteria for antagonism or pathogenesis by injecting toxins into target bacterial or eukaryotic cells [1-3]. T6SS is composed of a membrane complex in connection to a baseplate, which is the docking site for polymerization of a tube surrounded by a contractile sheath [4]. The tube is a puncturing device stacked of Hcp protein hexamer tipped with the trimeric Valine-glycine repeat protein G (VgrG) spike and a PAAR repeat-containing protein which sharpens the tip [5]. When the sheath contracts, the

72 puncturing device carrying effectors is propelled towards the target cell to deliver
73 effectors. After firing, the sheath disassembles and the subunits of the sheath are
74 recycled to build another machine [6].
75
76 In terms of delivery, the T6SS effectors can be classified as cargo or specialized
77 effectors. The cargo effectors interact non-covalently with Hcp, VgrG or PAAR while
78 in specialized effectors, the effector domain is covalently fused to Hcp, VgrG or PAAR
79 [7]. Functionally, most of the identified effectors mediate antibacterial activities
80 including nuclease, peptidoglycan hydrolase, lipase, phospholipase, NAD(P)+-
81 glycohydrolase and ADP ribosyltransferase by targeting conserved cellular structures
82 such as nucleic acids, peptidoglycan, and inner membrane as well as specific
83 metabolites or proteins [8, 9].
84
85 To date, the characterized T6SS nuclease effectors include members of HNH, N-Tox,
86 Tox-Rease, and PoNe superfamilies and were shown to target DNA substrates without
87 specificity [10-16]. Thus, expression of these T6SS nuclease effectors causes DNA
88 degradation *in vitro* and/or *in vivo*. Interestingly, the majority of T6SS DNase effectors
89 belong to HNH/ENDO VII nuclease superfamily, also named as His-Me finger
90 endonuclease superfamily consisting of 38 distinct families [17, 18]. These nuclease
91 superfamily proteins harbor three conserved His-Asp-His within a ~30-amino-acid
92 domain formed by a β1 hairpin followed by an α-helix to form a ββα-metal topology
93 for DNA binding and hydrolysis [17, 18]. Several T6SS effectors belonging to this
94 HNH/His-Me superfamily have been identified, including Tse7 of *Pseudomonas*
95 *aeruginosa* as Tox-GHH2 [15], Tse1 of *Aeromonas dhakensis* [13], V2a of
96 *Agrobacterium tumefaciens* as Tox-AHH [11], and two Tox-SHH family effectors Tke4
97 of *Pseudomonas putida* [19] and Txe4 of fish pathogen *Pseudomonas plecoglossicida*
98 [20]. Amino acid substitution experiments on Tse7, V2a, and Tse1 have indicated that
99 this conserved catalytic site [A/G]HH is required for the nuclease activity and toxicity
100 [11, 13, 15]. However, the impact of SHH and HNH motifs of the Tox-SHH family
101 effectors in nuclease activity and T6SS toxicity have not been demonstrated.
102
103 *A. tumefaciens* is a Gram-negative Alphaproteobacteria belonging to the
104 *Rhizobiaceae* family. It is an economically important pathogen that causes crown gall
105 disease and a gene delivery tool with capability of transforming plant cells and fungi

106 [21]. T6SS main gene cluster is highly conserved in the genome of *A. tumefaciens*
107 genomospecies complex [22-24]. Besides the main cluster consisting of two divergent
108 operons, *imp* (imp aired in nitrogen fixation) encoding core structural and regulatory
109 components and *hcp* operon for effectors and effector delivery components (e.g. Hcp,
110 VgrG, PAAR). Most *A. tumefaciens* strains also encode additional *vgrG* operons
111 encoding effector-immunity (EI) gene pairs. *A. tumefaciens* strain 1D1609 encodes
112 four *vgrG* genes (*vgrGa, vgrGb, vgrGc, vgrGd*) with each *vgrG* module associated with
113 three to four associated genes, named as *vgrG-associated* gene 1-4 in cluster *a/b/c/d*
114 [11]. Each *vgrG* gene is genetically linked to a conserved chaperone/adaptor gene
115 and different known or putative EI pairs, including three effectors with a conserved N-
116 terminal PAAR-like DUF4150 domain but distinct C-terminal effector domains (V2a,
117 V2c, and V2d) [11] (**Figure S1**). For *vgrGb* module, V2b does not encode an effector
118 domain but downstream two genes encode a putative ADP-ribosylating enzyme (V3b)
119 and a Rhs-linked effector domain (V4b), followed by a putative immunity. Previous
120 study by deletion of single or multiple EI pairs suggested that *vgrGa-associated*
121 effector V2a, a DNase effector harboring C-terminal Tox-AHH domain, appears to be
122 the major antibacterial toxin but *vgrGd-associated* effector V2d also contributes to full
123 antibacterial activity for 1D1609 against *Escherichia coli* prey [11]. The biochemical
124 and biological functions of other putative effectors encoded in the other three orphan
125 *vgrG* modules remain uncharacterized.
126
127 In this study, we discovered that *vgrGc*-associated effector V2c is a Tox-SHH DNase
128 toxin and explored the rationale of having two T6SS DNase toxins in *A. tumefaciens*
129 strain 1D1609. We show that the expression of V2c caused growth inhibition, plasmid
130 DNA degradation and cell elongation, which the phenotypes are neutralized by co-
131 expression of the cognate immunity protein, V3c. We also show that the SHH motif is
132 responsible for the nuclease activity of V2c. Importantly, V2a AHH nuclease and V2c
133 SHH nuclease exert different antibacterial capacities against specific bacterial
134 competitors and function synergistically to exert stronger antibacterial activity against
135 the soft rot phytopathogen, *Dickeya dadantii*. Harboring two classes of His-Me finger
136 nuclease effectors with potential target-specific toxicity may grant 1D1609 with
137 versatile antibacterial weapons in facing different bacterial competitors in microbial
138 community.

139 **RESULTS**

140 **V2c is a DNase belonging to the Tox-SHH clade of His-Me finger superfamily**
141 In 1D1609, *vgrGa*-associated effector V2a appears to be the major antibacterial toxin
142 against *Escherichia coli* prey [11]. V2c is a putative PAAR (DUF4150)-linked
143 specialized effector (**Figure 1A**) but the presence or absence of *v2c* did not affect the
144 antibacterial activity of 1D1609 against *E. coli* prey [11]. Aside from the N-terminal
145 PAAR domain, V2c does not show any sequence similarity to V2a (**Figure S2**). BLAST
146 and CDD searches did not identify known or conserved domain at its C-terminal region.
147 However, multiple sequence alignment of V2c and V2c orthologs revealed conserved
148 SHH and HNH motifs at the C-terminal region (**Figure 1B**). These V2c orthologs all
149 harbor C-terminal Tox-SHH domain but their N-terminal region can be fused to other
150 known T6SS domains such as Found in type sIX effector (FIX), DUF4150/PAAR-like
151 domain and Rhs core domain ([25], **Figure 1C).** Using the protein homology detection
152 program HHpred [26], we found that the C-terminal region of V2c encodes two parallel
153 β-strands connected by α-helix, which is signature structure in His-Me finger nuclease
154 [17]. Consistent with the result of secondary structure prediction, 3D structure
155 prediction using AlphaFold ([27, 28], **Figure 1D**) shows this domain consists of two
156 antiparallel β-strands connected with an Ω loop with a His (H384) at the C-terminus of
157 the first β-strand and followed by an α-helix, featuring a HNH motif of His-Me finger
158 endonuclease [17, 18]. These suggest V2c belongs to the Tox-SHH (Pfam PH15652)
159 clade of His-Me finger superfamily.
160
161 To determine the antibacterial and DNase activities of V2c, we expressed *v2c* using
162 an arabinose inducible promoter to determine if V2c is a bacterial toxin functioning as
163 a nuclease. Growth inhibition measured by optical density was observed when *v2c* is
164 expressed by arabinose induction in *Escherichia coli* and this can be neutralized by
165 co-expression of its putative cognate immunity *v3c* as compared to the vector control
166 (**Figure 2A**). Also, colony forming unit (CFU) count shows the reduced CFU of *v2c*-
167 expressed cells and higher CFU could be recovered with co-expression of *v3c* (**Figure**
168 **2B**). In addition, plasmid degradation assay showed that the expression of *v2c* upon
169 arabinose induction resulted in degradation of plasmid DNA in *E. coli* and this is
170 abolished when *v3c* is co-expressed (**Figure 2C**). The data indicated that V2c exhibits
171 DNase activity *in vivo*.

172

173 We further investigated whether the SHH and HNH motifs are involved in DNase
174 activity. His-Me finger superfamily has a strictly conserved His residue and catalytic
175 metal ion which are both essential for nucleic acid hydrolysis. Based on this premise,
176 we define a region spanning amino acid residues 380-409 as a His-Me finger domain
177 core region (CR). Based on the alignment, H384 is the catalytic His and H408 is for
178 metal ion binding while H383 may function as second residue for metal ion
179 coordination. To verify their roles in antibacterial and DNase activity, a series of
180 deletion as well as single and double amino acid substitution variants were generated.
181 Strikingly, no growth inhibition and plasmid degradation were observed in any of the
182 mutants expressing the CR deletion (V2c^{CR}), single (V2c^{H383A}, V2c^{H384A} and V2c^{H408A})
183 and double (V2c^{HAHA} substitution in both H383 and H384) variants (**Figure 2A, C, D**).
184 Higher CFU was also recovered from *E. coli* culture expressing these mutants alone
185 or with *v3c* (**Figure 2B**). To further confirm the DNase activity of V2c*,* each of V2c and
186 its variants is fused with 6x-His and purified for *in vitro* DNase activity assay. The
187 results showed that purified V2c fraction is able to degrade DNA, but not the eluate
188 from *E. coli* expressing the vector (pET28a) (**Figure 2D**). Consistent with the *in vivo*
189 plasmid degradation assay, no activity could be detected from V2c^{H384A}*,* V2c^{H408A}, or
190 V2c^{HAHA} variants. However, purified V2c^{H383A} fraction exhibited DNase activity by
191 degrading the plasmid DNA substrate. Western blot analysis of the reaction samples
192 shows V2c and its variants used for the assay were at similar protein levels. Taken the
193 results of *in vivo* and *in vitro* DNA degradation assays, the conserved H384 and H408
194 in the HNH motif are crucial for V2c DNase activity whereas H383 in SHH motif
195 appears to be less critical for *in vitro* but may be required for *in vivo* nuclease activity.

196 **Ectopic expression of V2c caused DNA degradation and cell elongation**

197 We next examined the cell morphology and DNA integrity of *E. coli* cells expressing
198 *v2c* and the two variants (*v2c^{CR}* and *v2c^{HAHA}*) that are defective in DNase activity and
199 toxicity. Cell morphology was observed by phase contrast while bacterial cell
200 membrane and DNA were stained by FM-4-64 and Hoechst, respectively under
201 fluorescence microscope. Hoechst signals are significantly reduced when *v2c* is
202 expressed by arabinose induction in *E. coli* and this can be rescued by co-expression
203 of its cognate immunity *v3c* shown in the images and quantification (**Figure 3A, B**).
204 Hoechst signals are diminished only in *E. coli* cells producing *v2c* but not *v2c*^{HAHA},

205 *v2c*^{CR} and vector control, suggesting that the cellular DNA degradation is caused by
206 V2c DNase activity, which can be neutralized by its immunity protein V3c. In addition,
207 we also observed cell elongation in *E. coli* expressing *v2c* and co-expression of *v3c*
208 rescues the cell elongation phenotype (**Figure 3A, C**). However, *E. coli* cells
209 expressing *v2c*^{CR} and *v2c*^{HAHA} as well as other single amino acid substitution variants
210 (*v2c*^{H383A}, *v2c*^{H384A}, *v2c*^{H408A}) do not abolish the elongated cell phenotype (**Figure 3A,**
211 **C, Figure S3A, B**).

212 **Ectopic expression of V2a also caused cell elongation phenotype**

213 Previous study showed that V2a is a Tox-AHH nuclease that serves as the major
214 antibacterial weapon in 1D1609 [11]. H385 and H386 are two of the predicted His
215 residues in AHH motif of V2a, corresponding to H383 and H384 in SHH motif of V2c.
216 The structure predicted by AlphaFold indicates V2a also features a His-Me finger,
217 having two α-helices with histidine residues (H430, H456) followed by the β-strands
218 (**Figure 4A**). Previous findings demonstrated that the expression of *v2a* but not
219 *v2a*^{H385A} caused growth inhibition and plasmid degradation in *E. coli* [11]. To gather
220 further insight of V2a AHH motif in the His-Me finger domain, we evaluated the
221 growth and morphology of arabinose induced *v2a* mutants. Results show that the
222 expression of *v2a* caused reduction in Hoechst-stained DNA signals and resulted in
223 cell elongation (**Figure 4B, C, D**). The expression of *v2a*^{H385A} has similar levels of
224 Hoechst-stained DNA signals and cell length as compared to the vector control.
225 These results suggest that the cell elongation phenotype observed were caused by
226 V2a DNase activity, whereas V2c shows DNase activity-independent cell elongation.
227 We also determined the toxicity of another putative effector V4b of 1D1609, a PAAR
228 (DUF4150)-linked specialized effector but harboring a Rhs domain with structural
229 similarity to the insecticidal toxin [11] (**Figure S4A**). Expression of *v4b* caused
230 growth inhibition in *E. coli,* in which the growth inhibition can be rescued by co-
231 expression of its putative cognate immunity *v5b* to a level similar to vector control
232 (**Figure S4B**). However, no DNA degradation and cell elongation could be observed
233 (**Figure S4C, D, E, F**). These results show that V4b is a bacterial toxin and V5b is
234 the cognate immunity protein and suggest that cell elongation phenotype may be
235 specific to toxicity of nuclease effectors.

236 **V2c nuclease exhibits antibacterial activity at both intra-species and inter-**
237 **species competition and functions synergistically with V2a against the soft rot**
238 **phytopathogen, *Dickeya dadantii***
239 To correlate the DNA degradation and cell elongation phenotypes observed by ectopic
240 expression of *v2c* in *E. coli* in a more biologically relevant context, we further
241 performed interbacterial competition assay. We first selected *A. tumefaciens* strain
242 C58, which possess incompatible EI pairs with 1D1609 and previously demonstrated
243 to be susceptible to 1D1609 T6SS killing [22], for intra-species competition. Each of
244 1D1609 mutants lacking multiple EI pairs attackers was co-cultured with C58 strain
245 harboring pRL-GFP(S65T) prey *in vitro* on AK agar [29] and the number of viable C58
246 prey cells ($\log_{10}$ CFU/mL) were quantified. Similar to previous killing assay using *E.*
247 *coli* prey [11], we detected ~ 2 log of reduced prey cell survival by 1D1609 WT attacker,
248 as compared to the Δ*4EI* mutant with deletion of all four EI pairs (**Figure 5A**). Other
249 double *(*Δ*EIbd*) or triple deletion mutants (Δ*EIabd,* Δ*EIbcd*) exhibited compromised but
250 detectable antibacterial activity to C58, indicating that *v2a* or *v2c* alone is sufficient to
251 exhibit antibacterial activity to C58.
252
253 Intrigued by the observation that *v2c* could exhibit antibacterial activity to *A.*
254 *tumefaciens* C58 prey but no significant effect against *E. coli* prey [11], we reasoned
255 that *E. coli* may not be physiologically relevant prey for *Agrobacterium* although *v2c* is
256 able to cause toxicity when directly expressed in *E. coli* (**Figure 2A, B**). We then
257 selected *Dickeya dadantii* as the prey cells for inter-species competition because it is
258 a phytopathogen but also a close relative of *E. coli*, both belonging to
259 *Enterobacteriaceae*. To avoid potential counterattack by *D. dadantii* T6SS [30], a
260 T6SS-deficient mutant, Δ*imp* with deletion of *imp* operon, harboring pRL-GFP(S65T)
261 (*D. dadantii* Δ*imp*-GFP(S65T)) was used as a prey. CFU counting of *D. dadantii* Δ*imp*-
262 GFP(S65T) prey cells after co-culture show that ~ 1.5 log of reduced prey cell survival
263 by 1D1609 WT attacker, as compared to the Δ*4EI* mutant (**Figure 5B**). The presence
264 of *v2a* only (Δ*3EIbcd*) exhibited comparable antibacterial activity as the WT while *v2c*
265 only (Δ*3EIabd*) showed weak but detectable antibacterial activity as compared to Δ*4EI,*
266 indicating *v2c* itself is able to kill *D. dadantii* but with much weaker activity than *v2a*.
267 Strikingly, 1D1609 expressing both *v2a* and *v2c* (Δ*2EIbd*) could result in stronger
268 killing effects than WT. The use of pRL-GFP(S65T) with constitutive expression of
269 GFP also allowed us to observe the *D. dadantii* Δ*imp*-GFP(S65T) prey cells under the

270 fluorescence microscope after co-culture. We observed very few cells expressing GFP
271 when competing with WT or Δ*3EIbcd* expressing *v2a* only. The lysed and elongated
272 *D. dadantii* cells were also detected when co-cultured with 1D1609 with either strains
273 expressing *v2a* only (Δ*3EIbcd*), *v2c* only (Δ*3EIabd*), or both Δ*3EIbd* (**Figure 5C**). We
274 further quantified the cell length of GFP-expressing *D. dadantii* cells. The results show
275 that majority of cells were elongated after 18 hours of co-culture with 1D1609
276 expressing either *v2a* (Δ*3EIbcd*) or *v2c* (Δ*3EIabd*), or combination of both (Δ*3EIbd*),
277 as compared to those *D. dadantii* cells alone or co-incubated with Δ*4EI* (**Figure 5D**).
278
279 Taken together, these results suggest that V2c nuclease exhibits antibacterial activity
280 at both intra-species and inter-species competition but at different capacities. While
281 V2a and V2c exert similar antibacterial against *A. tumefaciens* C58, V2c only exhibits
282 weak antibacterial activity but functions synergistically with V2a when competing with
283 *D. dadantii* prey, resulting to elongated and lysed cells.

284 **DISCUSSION**

285 His-Me finger nucleases are a large and diverse superfamily of nucleases; however,
286 only a limited number of T6SS effectors have been identified as His-Me finger
287 nuclease. In the present study, we reported that *A. tumefaciens* strain 1D1609
288 encodes two His-Me finger superfamily DNases, V2a and V2c belonging to Tox-AHH
289 and Tox-SHH family respectively, exhibiting different capacities to specific bacterial
290 competitors.
291
292 His-Me finger nucleases are one-metal-ion-dependent nucleases, primarily dependent
293 on Mg^{2+} or in some cases dependent on Zn^{2+}. The only invariant residue in His-Me
294 endonuclease is the catalytic His located at the end of β1 strand (1st H in HNH motif,
295 H384 for V2c and H386 for V2a, **Figure 1D, 4A, S2)**, which functions as the general
296 base for hydrolysis of phosphodiester bonds. The other conserved His (last H in HNH
297 motif, H408 for V2c and H430 for V2a) and Asn/Asp/Glu/His located before the
298 invariant His (H383 for V2c and H384 for V2a) are involved in coordinating the single
299 metal ion. Indeed, our data show that H383, H384, and H408 of V2c and H385 and
300 H386 of V2a are required for exerting DNase activity *in vivo* (**Figure 2C,** [11]. However,
301 different from the loss of DNase activity *in vivo* and *in vitro* for both V2c^{H384A} and

302 V2c^{H3408A}, V2c^{H383A} variant retains the DNase activity by an *in vitro* nuclease activity
303 assay (**Figure 2D**). This indicates the requirement of H383 in coordinating metal ion
304 binding for DNase activity may be subject to environmental factors.
305
306 His-Me finger encodes a small structural motif, so it is usually associated with other
307 domain architectures that could play additional functions. In addition, its three-element
308 structural motif is unable to provide enough of a hydrophobic core for stability [18].
309 Thus, many proteins containing the His-Me finger employ a variety of additional
310 structural elements or domains for stabilization and/or specificity. V2c and its orthologs
311 commonly found in *Rhizobiaceae* are not included in the reported 77 sequences with
312 conserved core regions of His-Me finger superfamily [18]. Our evidence further
313 suggests that V2c may represent a new branch of Tox-SHH toxin family (Pfam
314 PF15652), which includes proteins with additional domain architectures (**Figure 1C**).
315 These additional domain(s) are conserved regions found in many bacterial toxin
316 proteins and may facilitate the secretion of nuclease and affect its toxicity to the
317 competing cell. While both V2c and V2a harbor the conserved N-terminal DUF4150
318 PAAR-like domain, they share low sequence similarity in the C-terminal His-Me finger
319 domain (**Figure S2**), in which the protein structures predicted by AlphaFold reveal the
320 structural difference between V2c and V2a (**Figure 1C, 4A**). This discrepancy may
321 contribute to the difference on toxicity strength and the role of DNase on cell elongation.
322 Alternatively, V2a and V2c may have the same mechanism to bind and hydrolyze DNA
323 for toxicity and the difference in the phenotype is caused by another domain outside
324 the His-Me finger fold.
325
326 Cell elongation could still be observed in the *E. coli* strain carrying different DNase
327 defective *v2c* variants, even in the absence of arabinose (**Figure 3A, B, S2A**). Several
328 studies reported the leaky expression of T6SS toxin driven by arabinose-inducible
329 P_{BAD} promoter resulted in toxicity in the absence of arabinose [16, 25]. Thus, we
330 speculated that the leaky expression of these *v2c* variants is sufficient to induce the
331 cell elongation phenotype. The data suggest that another domain outside the SHH
332 catalytic region in V2c is responsible for the cell elongation phenotype. This is different
333 from the nuclease activity-dependent filamentation observed previously [15, 31] and
334 V2a (**Figure 4**), suggesting that V2c-induced cell elongation is independent of
335 nuclease activity. The proposed biological role of bacterial filamentation is mainly

336 related to stress response to thrive for survival [32]. One of the conditions that lead to
337 filamentation is DNA damage. When the DNA is damaged, the SOS response is
338 induced and cells may delay the cell cycle and inhibit cell division until DNA repair and
339 replication are complete. Although V2c catalytic site variants lose activity for DNA
340 cleavage, they may still bind to DNA and induce cell elongation. Furthermore, cell
341 division arrest could be also caused by non-nuclease effectors. For example, a T6SS
342 ADP-ribosyltransferase effector called Tre1 in *Serratia proteamaculans* was reported
343 to inactivate bacterial cell division Tre1 by modifying arginine on FtsZ to block
344 polymerization [33]. Future work by domain dissection of V2c is needed to identify the
345 domain causing cell elongation.
346
347 While HNH/His-Me T6SS nucleases are the most prevalent nuclease toxins identified
348 in T6SS, most bacterial genomes only encode one type of HNH/His-Me nuclease
349 effector, including Tse7 of *P. aeruginosa* [15], Tse1 of *A. dhakensis* [13], and Tke4 of
350 *P. putida* [19]. Besides *A. tumefaciens* 1D1609 encoding Tox-AHH (V2a) and Tox-
351 SHH (V2c) nucleases, the use of multiple HNH/His-Me nucleases as T6SS
352 antibacterial weapons have been identified in fish pathogen *P. plecoglossicida* [20]. *P.*
353 *plecoglossicida* T6SS-2 mediates interbacterial competition and encodes four putative
354 effectors, all contain C-terminal toxin domains belonging to HNH/His-Me superfamily
355 but distinct classes (Txe1 with a dipeptide HH motif, Txe2 as Tox-AHH, Txe3 with
356 HNHc, and Txe4 as Tox-SHH) [20]. Among them, Txe1, Txe2, and Txe4 exhibit *in vitro*
357 nuclease activity and toxicity when expressed in *E. coli*. However, only Txe1 and Txe4
358 contributes to interbacterial activity against *E. coli,* with Txe1 as the predominant toxin,
359 in which its C-terminal conserved dipeptide HH motif is required for nuclease activity
360 and toxicity to *E. coli.* Txe4 is also required for full interbacterial competition but the
361 role of SHH motif in DNase and toxicity has not been determined. Together with our
362 findings, it is possible that having multiple distinct or same classes of nuclease
363 effectors may provide versatile toxicity when competing with different preys, in which
364 some toxins may only exhibit activity against specific preys.
365
366 The strain 1D1609 is unique in *A. tumefaciens* species complex with multiple VgrG
367 spikes carrying different antibacterial effectors [11] . Our findings that *v2a* and *v2c*
368 exhibit different capacities against different preys support previous studies that some
369 T6SS toxins can only exert toxicity in specific bacterial species [23, 34]. From the

370 observation of the synergism of V2a and V2c against *D. dadantii,* harboring multiple
371 T6SS effectors in 1D1609 may provide an advantage for the strain to maintain a
372 growth competitiveness in different niches and environments.

373 MATERIALS AND METHODS

374 Bacterial strains and growth conditions

375 Bacterial strains and plasmids are listed in Table S1. *Escherichia coli* strains were
376 grown in Luria-Bertani (LB) medium at 37°C, *A. tumefaciens* strains in 523 medium at
377 25°C and *D. dadantii* 3937 in LB medium at 30°C. Antibiotics were added when
378 necessary: for *E. coli*, 30 µg/mL gentamicin and 250 µg/mL streptomycin; for *D.*
379 *dadantii* and *A. tumefaciens,* 50 µg/mL gentamicin.
380

381 Molecular cloning

382 Plasmid pJN105 was used for expression of toxin genes and pTrc200 plasmid was
383 used for expression of immunity gene. PCR was amplified with KAPA HiFi HotStart
384 DNA Polymerase (Roche, Switzerland) using genomic DNA of *A. tumefaciens* 1D1609.
385 The primers used in the study are listed in Table S2. Site directed mutagenesis was
386 done using either DpnI or Gibson Assembly (New England BioLabs, USA), ligated
387 using T4 ligase (Takara) and transformed into chemically competent *E. coli* DH10B.
388 Plasmid DNA was isolated using QIAprep miniprep kit (Qiagen, Germany). All
389 constructs were confirmed by sequencing. The in-frame deletion mutants in *A.*
390 *tumefaciens* were generated using a suicide plasmid via double crossing over by
391 electroporation or by conjugation as described [11].

392 Bioinformatic analysis

393 The orthologs of V2c were analyzed using amino acid sequences after the DUF4150
394 domain via BLASTP search. Multiple sequence alignment was performed using
395 MUSCLE or Multiple Sequence Comparison by Log- Expectation [35]. Full length
396 sequences of the V2c orthologs were analyzed to obtain domain architectures from
397 Pfam database [36]. The E-value threshold was set at 10^{-5}. HHpred [26] and Swiss
398 Model [37] were used for homology-based protein structure prediction. Protein
399 structure was predicted by AlphaFold [27, 28] from the UniProt database. Secondary
400 structure prediction was done using default settings in PSIPRED 4.0 Protein
401 Structure Prediction Server/ DMPfold 1.0 Fast Mode [38, 39].

402 **Growth inhibition assay**

403 Growth inhibition assay was performed as described previously [10]. In brief, overnight
404 cultures of *E. coli* DH10B strain with empty vectors (pJN105 for effector gene and
405 pTrc200 for immunity gene) or the derivatives were adjusted to OD_{600} of 0.1 in LB
406 medium. 1 mM isopropyl β-D-1- thiogalactopyranoside (IPTG, Amresco) was used to
407 induce the expression of the putative immunity protein. After 1 hour of IPTG induction,
408 L-arabinose (Ara, Sigma-Aldrich) was added to 0.2% final concentration, to induce
409 expression of the toxin. Cell growth was recorded every hour at OD_{600}. Empty vectors
410 were used as controls. After 8 hours, cells were harvested to quantify the number of
411 colony forming units (log_{10} CFU/mL) by automatic diluter and plater, easySpiral Dilute
412 (Interscience, France).
413

414 **Plasmid DNA degradation analysis in *E. coli* cells**

415 *In vivo* plasmid DNA degradation analysis was performed as described previously [10].
416 In brief, overnight cultures of *E. coli* DH10B strain with empty vectors (pJN105 for
417 effector gene and pTrc200 for immunity gene) or the derivatives grown in LB broth
418 were harvested and adjusted to OD_{600} ~0.3 in LB medium. *E. coli* cultures were
419 induced with 1 mM IPTG at 0 hour for *v3c* expressed from pTrc200 plasmid followed
420 by L-arabinose (0.2%, final concentration) induction at 1 hour to induce *v2c* from
421 pJN105 plasmid and cultured for 2 hours. Equal amounts of cells were used for
422 plasmid DNA extraction and equal volume of extracted DNA was resolved in agarose
423 gel followed by ethidium bromide staining and visualized using Gel Doc XR+ UV Gel
424 Documentation Molecular Imager Universal Hood II (Bio-Rad, USA).

425 **Cloning, expression and purification of V2c and mutants**

426 For *in vitro DNase* activity assay, the effector gene *v2c* was constructed in pET28a
427 plasmid and immunity gene *v3c* was constructed in pTrc200 plasmid. Site-directed
428 mutagenesis was done by using overlap extension PCR. Plasmid for expressing
429 effector protein, *v2c* or its variants, and plasmid for expressing immunity protein, *v3c*,
430 were transformed into *E. coli* BL21(DE3) for IPTG-induced co-expression. Bacterial
431 culture was incubated at 37 °C until OD_{600} reached 0.5, then 0.1 mM IPTG was added
432 followed by 5-h expression at 37°C. Pellets were collected, sonicated, and expressed
433 proteins were purified by using Ni Sepharose 6 Fast Flow histidine-tagged protein

434 purification resin (Cytiva, Germany). Briefly, cells were lysed in extraction buffer (50
435 mM Tris-Cl, pH7.5, 0.1 M NaCl, 20 mM imidazole) and proteins were eluted by using
436 elution buffer with up to 250 mM imidazole in 50 mM Tris-Cl, pH7.5, 0.1 M NaCl.

437 ***In vitro* DNase activity assay**

438 A 10 µL reaction containing 200 ng of pTrc200HA plasmid DNA and 1× CutSmart
439 Buffer (New England BioLabs, USA) with partially purified V2c or its variants
440 normalized by the major V2c protein band was incubated at 37°C for 1 hour. The
441 digestion of DNA was determined by agarose gel electrophoresis and visualized by
442 SYBR Safe DNA gel stain (Invitrogen, USA). The reaction samples of V2c or its
443 variants were scaled up for Western blotting analysis. Anti-V2c antibody was
444 generated in rabbits against two V2c peptides, PFYWDFPNSQVGRD and
445 KRIAMLRGDPTRYD (indicated in Figure S1) by Yao-Hong Biotechnology Inc.
446 (Taiwan).

447 **Western blot analysis**

448 Western blot analysis was performed as described [40]. In general, proteins were
449 resolved by SDS-PAGE and transferred onto a PVDF membrane by using a transfer
450 apparatus (Bio-Rad, USA). The membrane was probed with primary antibody against
451 V2c (1:4000), Hcp (1:2500), TssB (1:4000) and GFP (1:1000), followed by incubation
452 with horseradish peroxidase-conjugated anti-rabbit secondary antibody (Chemichem)
453 (1:25000) and visualized with the ECL system (Perkin-Elmer Life Science, Boston,
454 USA).

455 **Fluorescence microscopy and image analysis**

456 *E. coli* DH10B carrying the empty vectors (pJN105 for effector gene and pTrc200 for
457 immunity gene) or the derivatives were grown overnight at 37°C. Overnight cultures
458 were sub-cultured with OD_{600} ~0.01. After 1 hour, L-arabinose (Ara) was added (0.2%
459 final concentration) to induction. Cultures were harvested after an hour and
460 resuspended with 30 µL PBS with 0.5 % Tween 20 (PBST). Three µL of cells was
461 placed on 2% agarose pad and imaged. To check the DNA degradation, the same
462 protocol was followed and live cells were stained with 2 µg/mL Hoechst (Life
463 Technologies, USA) and 1 µg/mL FM4-64FX, fixable analog of FM-4-64 (Invitrogen,
464 USA) for 5 mins and washed with PBS to remove the excess dye.
465

466 For co-culture of *D. dadantii* Δ*imp*-GFP(S65T) with various 1D1609 EI pair mutants,
467 strains were mixed at 1:10 ratio on AK agar, *Agrobacterium* kill-triggering (AK) medium
468 (3 g K_2HPO_4, 1 g NaH_2PO_4, 1 g NH_4Cl, 0.15 g KCl, 9.76 g MES in 900 mL ddH_20, pH
469 5.5) [29] solidified by 2% (w/v) agar. Cells from 16 hour co-culture at 25°C were
470 concentrated to OD_{600} ~10 and spotted on 2% agarose pad for imaging.
471
472 Imaging was performed using an inverted fluorescent microscope (IX81, Olympus
473 Japan) with objective lens UPLSAPO 100XO (Olympus, Tokyo, Japan), DAPI (49000;
474 Chroma), GFP (49002; Chroma) and Cy3 (49005; Chroma) filter set and CCD camera
475 (ORCA-R2; Hamamatsu, Japan). The images were acquired using Olympus cellSens
476 Dimension software.
477
478 All the image analysis was done using Fiji analyze particles tool [41]. The micrograph
479 of FM-4-64 fluorescence was used to segment surfaces (i.e. individual bacterial cell)
480 with background subtraction and thresholding. Feret's diameter was used. The cell
481 length (μm) was determined from cumulative counts of three random frames per
482 sample. For quantification of cell degradation, the Hoechst intensity was normalized
483 using the formula intensity/unit area of cells, where intensity is major x minor x 3.14
484 (π).

485 **Interbacterial competition assay**

486 Bacterial competitions were carried out as described [22] with modifications. Briefly,
487 overnight culture of *A. tumefaciens* and *D. dadantii* 3937 Δ*imp* were mixed at a 10:1
488 attacker to prey ratio and spotted on Agrobacterium kill-triggering (AK) agar plates [29].
489 The prey *A. tumefaciens* C58 or *D. dadantii* 3937 Δ*imp* was transformed with pRL662-
490 GFP(S65T) for gentamycin selection or microscopy imaging. After 18 hour incubation
491 at 25°C, the co-cultured cells were collected, serially diluted and plated on LB agar
492 containing gentamicin to quantify surviving prey cells by counting CFU.

493 **Statistical analysis**

494 The statistical analyses were done using GraphPad Prism version 6.01 for Windows,
495 GraphPad Software, La Jolla California USA (www.graphpad.com). The number of
496 technical replicates and independent biological replicates, p values and statistical
497 tests performed are indicated in the figure legends. The mean of independent

replicates was compared using the following statistical tests: Student's t test, one-way ANOVA followed by Tukey's multiple comparisons tests (http://astatsa.com/OneWay_Anova_with_TukeyHSD/). The error bars indicate the standard error of the mean (SEM).

ACKNOWLEDGEMENTS

The authors acknowledge Ching-Hong Yang for providing *Dickeya dadantii* 3937 strains, which were imported under the permit 106-B-003 issued by the Council of Agriculture of Taiwan. We would like to thank the former and current Lai lab members for their help and fruitful discussion throughout this study, as well as See-Yeun Ting and Mao-Sen Liu for critically reading the manuscript and their valuable comments. We also thank Venus Marie Gaela and Thomas Boudier for the guidance and help in processing the images using Fiji and the Sanger DNA sequencing service provided by Genomic Technology Core located at the Institute of Plant and Microbial Biology, Academia Sinica. The funding was supported by grants National Science and Technology Council (NSTC) of Taiwan (107-2311-B-001-019-MY3) and Academia Sinica Investigator Award (AS-IA-107-L01) to EML, and NSTC grant (110-2311-B001-011) to YLS. YWC was supported by the postdoctoral fellowship (NSTC 110-2811-B-001-504). The funders had no role in study design, data collection and interpretation, or the decision to submit the work for publication.

AUTHOR CONTRIBUTION

Conceptualization: MNMS, EML; Investigation: MNMS, KP, PYH, YWC, LKS, YLS, EML; Project Funding acquisition and administration: EML, YLS; Supervision: EML, YLS; Writing of original draft: MNMS, EML; Writing – methodology, review & editing: MNMS, KP, PYH, YWC, LKS, YLS, EML.

REFERENCES

1. Hood RD, Peterson SB, Mougous JD. From Striking Out to Striking Gold: Discovering that Type VI Secretion Targets Bacteria. Cell Host Microbe. 2017;21(3):286-9. doi: 10.1016/j.chom.2017.02.001. PubMed PMID: 28279332.

526 2. Coulthurst S. The Type VI secretion system: a versatile bacterial weapon.
527 Microbiology (Reading). 2019;165(5):503-15. Epub 2019/03/21. doi: 10.1099/mic.0.000789.
528 PubMed PMID: 30893029.

529 3. Hachani A, Wood TE, Filloux A. Type VI secretion and anti-host effectors. Curr Opin
530 Microbiol. 2016;29:81-93. Epub 2016/01/02. doi: 10.1016/j.mib.2015.11.006. PubMed
531 PMID: 26722980.

532 4. Wang J, Brodmann M, Basler M. Assembly and Subcellular Localization of Bacterial
533 Type VI Secretion Systems. Annu Rev Microbiol. 2019;73:621-38. Epub 2019/06/22. doi:
534 10.1146/annurev-micro-020518-115420. PubMed PMID: 31226022.

535 5. Shneider MM, Buth SA, Ho BT, Basler M, Mekalanos JJ, Leiman PG. PAAR-repeat
536 proteins sharpen and diversify the type VI secretion system spike. Nature.
537 2013;500(7462):350-3. Epub 2013/08/09. doi: 10.1038/nature12453. PubMed PMID:
538 23925114; PubMed Central PMCID: PMC3792578.

539 6. Basler M, Pilhofer M, Henderson GP, Jensen GJ, Mekalanos JJ. Type VI secretion
540 requires a dynamic contractile phage tail-like structure. Nature. 2012;483(7388):182-6. Epub
541 2012/03/01. doi: nature10846 [pii]

542 10.1038/nature10846. PubMed PMID: 22367545; PubMed Central PMCID: PMC3527127.

543 7. Cianfanelli FR, Monlezun L, Coulthurst SJ. Aim, Load, Fire: The Type VI Secretion
544 System, a Bacterial Nanoweapon. Trends Microbiol. 2016;24(1):51-62. doi:
545 10.1016/j.tim.2015.10.005. PubMed PMID: 26549582.

546 8. Lien YW, Lai EM. Type VI Secretion Effectors: Methodologies and Biology. Front Cell
547 Infect Microbiol. 2017;7:254. doi: 10.3389/fcimb.2017.00254. PubMed PMID: 28664151;
548 PubMed Central PMCID: PMC5471719.

549 9. Cherrak Y, Flaugnatti N, Durand E, Journet L, Cascales E. Structure and Activity of the
550 Type VI Secretion System. Microbiol Spectr. 2019;7(4). Epub 2019/07/13. doi:
551 10.1128/microbiolspec.PSIB-0031-2019. PubMed PMID: 31298206.

552 10. Ma LS, Hachani A, Lin JS, Filloux A, Lai EM. Agrobacterium tumefaciens deploys a
553 superfamily of type VI secretion DNase effectors as weapons for interbacterial competition
554 in planta. Cell Host Microbe. 2014;16(1):94-104. doi: 10.1016/j.chom.2014.06.002. PubMed
555 PMID: 24981331; PubMed Central PMCID: PMC4096383.

556 11. Santos MNM, Cho ST, Wu CF, Chang CJ, Kuo CH, Lai EM. Redundancy and Specificity
557 of Type VI Secretion vgrG Loci in Antibacterial Activity of Agrobacterium tumefaciens
558 1D1609 Strain. Frontiers in Microbiology. 2020;10. doi: ARTN 3004

559 10.3389/fmicb.2019.03004. PubMed PMID: WOS:000510643200001.

560 12. Ma J, Pan Z, Huang J, Sun M, Lu C, Yao H. The Hcp proteins fused with diverse
561 extended-toxin domains represent a novel pattern of antibacterial effectors in type VI
562 secretion systems. Virulence. 2017;8(7):1189-202. Epub 20170106. doi:
563 10.1080/21505594.2017.1279374. PubMed PMID: 28060574; PubMed Central PMCID:
564 PMCPMC5711352.

565 13. Pei TT, Li H, Liang X, Wang ZH, Liu G, Wu LL, et al. Intramolecular chaperone-
566 mediated secretion of an Rhs effector toxin by a type VI secretion system. Nat Commun.

567 2020;11(1):1865. Epub 20200420. doi: 10.1038/s41467-020-15774-z. PubMed PMID:
568 32313027; PubMed Central PMCID: PMCPMC7170923.

569 14. Fitzsimons TC, Lewis JM, Wright A, Kleifeld O, Schittenhelm RB, Powell D, et al.
570 Identification of Novel Acinetobacter baumannii Type VI Secretion System Antibacterial
571 Effector and Immunity Pairs. Infect Immun. 2018;86(8). Epub 20180723. doi:
572 10.1128/IAI.00297-18. PubMed PMID: 29735524; PubMed Central PMCID:
573 PMCPMC6056853.

574 15. Pissaridou P, Allsopp LP, Wettstadt S, Howard SA, Mavridou DAI, Filloux A. The
575 Pseudomonas aeruginosa T6SS-VgrG1b spike is topped by a PAAR protein eliciting DNA
576 damage to bacterial competitors. Proc Natl Acad Sci U S A. 2018;115(49):12519-24. Epub
577 2018/11/21. doi: 10.1073/pnas.1814181115. PubMed PMID: 30455305; PubMed Central
578 PMCID: PMCPMC6298103.

579 16. Fridman CM, Keppel K, Gerlic M, Bosis E, Salomon D. A comparative genomics
580 methodology reveals a widespread family of membrane-disrupting T6SS effectors. Nat
581 Commun. 2020;11(1):1085. Epub 20200227. doi: 10.1038/s41467-020-14951-4. PubMed
582 PMID: 32109231; PubMed Central PMCID: PMCPMC7046647.

583 17. Wu CC, Lin JLJ, Yuan HS. Structures, Mechanisms, and Functions of His-Me Finger
584 Nucleases. Trends Biochem Sci. 2020;45(11):935-46. Epub 20200814. doi:
585 10.1016/j.tibs.2020.07.002. PubMed PMID: 32807610.

586 18. Jablonska J, Matelska D, Steczkiewicz K, Ginalski K. Systematic classification of the
587 His-Me finger superfamily. Nucleic Acids Res. 2017;45(20):11479-94. doi:
588 10.1093/nar/gkx924. PubMed PMID: 29040665; PubMed Central PMCID: PMCPMC5714182.

589 19. Bernal P, Allsopp LP, Filloux A, Llamas MA. The Pseudomonas putida T6SS is a plant
590 warden against phytopathogens. ISME J. 2017;11(4):972-87. Epub 2017/01/04. doi:
591 10.1038/ismej.2016.169. PubMed PMID: 28045455; PubMed Central PMCID:
592 PMCPMC5363822.

593 20. Li Y, Yan X, Tao Z. Two Type VI Secretion DNase Effectors are Utilized for
594 Interbacterial Competition in the Fish Pathogen Pseudomonas plecoglossicida. Front
595 Microbiol. 2022;13:869278. Epub 20220406. doi: 10.3389/fmicb.2022.869278. PubMed
596 PMID: 35464968; PubMed Central PMCID: PMCPMC9020831.

597 21. Hwang HH, Yu M, Lai EM. Agrobacterium-Mediated Plant Transformation: Biology
598 and Applications: American Society of Plant Biologists; 2017.

599 22. Wu CF, Santos MNM, Cho ST, Chang HH, Tsai YM, Smith DA, et al. Plant-Pathogenic
600 Agrobacterium tumefaciens Strains Have Diverse Type VI Effector-Immunity Pairs and Vary
601 in In-Planta Competitiveness. Mol Plant Microbe In. 2019;32(8):961-71. doi: 10.1094/Mpmi-
602 01-19-0021-R. PubMed PMID: WOS:000477044200007.

603 23. Wu CF, Weisberg AJ, Davis EW, 2nd, Chou L, Khan S, Lai EM, et al. Diversification of
604 the Type VI Secretion System in Agrobacteria. mBio. 2021;12(5):e0192721. Epub
605 2021/09/15. doi: 10.1128/mBio.01927-21. PubMed PMID: 34517758; PubMed Central
606 PMCID: PMCPMC8546570.

607 24. Chou L, Lin YC, Haryono M, Santos MNM, Cho ST, Weisberg AJ, et al. Modular
608 evolution of secretion systems and virulence plasmids in a bacterial species complex. BMC

609 Biol. 2022;20(1):16. Epub 2022/01/14. doi: 10.1186/s12915-021-01221-y. PubMed PMID:
610 35022048; PubMed Central PMCID: PMCPMC8756689.

611 25. Jana B, Fridman CM, Bosis E, Salomon D. A modular effector with a DNase domain
612 and a marker for T6SS substrates. Nat Commun. 2019;10(1):3595. Epub 20190809. doi:
613 10.1038/s41467-019-11546-6. PubMed PMID: 31399579; PubMed Central PMCID:
614 PMCPMC6688995.

615 26. Soding J, Biegert A, Lupas AN. The HHpred interactive server for protein homology
616 detection and structure prediction. Nucleic Acids Res. 2005;33(Web Server issue):W244-8.
617 doi: 10.1093/nar/gki408. PubMed PMID: 15980461; PubMed Central PMCID:
618 PMCPMC1160169.

619 27. Jumper J, Evans R, Pritzel A, Green T, Figurnov M, Ronneberger O, et al. Highly
620 accurate protein structure prediction with AlphaFold. Nature. 2021;596(7873):583-9. Epub
621 20210715. doi: 10.1038/s41586-021-03819-2. PubMed PMID: 34265844; PubMed Central
622 PMCID: PMCPMC8371605.

623 28. Varadi M, Anyango S, Deshpande M, Nair S, Natassia C, Yordanova G, et al. AlphaFold
624 Protein Structure Database: massively expanding the structural coverage of protein-
625 sequence space with high-accuracy models. Nucleic Acids Res. 2022;50(D1):D439-D44. doi:
626 10.1093/nar/gkab1061. PubMed PMID: 34791371; PubMed Central PMCID:
627 PMCPMC8728224.

628 29. Yu M, Wang YC, Huang CJ, Ma LS, Lai EM. Agrobacterium tumefaciens Deploys a
629 Versatile Antibacterial Strategy to Increase its Competitiveness. J Bacteriol. 2020. Epub
630 2020/11/11. doi: 10.1128/JB.00490-20. PubMed PMID: 33168638.

631 30. Koskiniemi S, Lamoureux JG, Nikolakakis KC, t'Kint de Roodenbeke C, Kaplan MD,
632 Low DA, et al. Rhs proteins from diverse bacteria mediate intercellular competition. Proc
633 Natl Acad Sci U S A. 2013;110(17):7032-7. Epub 2013/04/11. doi: 1300627110 [pii]

634 10.1073/pnas.1300627110. PubMed PMID: 23572593; PubMed Central PMCID:
635 PMC3637788.

636 31. Yu M, Lai EM. Warfare between Host Immunity and Bacterial Weapons. Cell Host
637 Microbe. 2017;21(1):3-4. doi: 10.1016/j.chom.2016.12.012. PubMed PMID: 28081441.

638 32. Justice SS, Hunstad DA, Cegelski L, Hultgren SJ. Morphological plasticity as a bacterial
639 survival strategy. Nature Reviews Microbiology. 2008;6(2):162-8. doi: 10.1038/nrmicro1820.
640 PubMed PMID: WOS:000252426700015.

641 33. Ting SY, Bosch DE, Mangiameli SM, Radey MC, Huang S, Park YJ, et al. Bifunctional
642 Immunity Proteins Protect Bacteria against FtsZ-Targeting ADP-Ribosylating Toxins. Cell.
643 2018;175(5):1380-92 e14. Epub 20181018. doi: 10.1016/j.cell.2018.09.037. PubMed PMID:
644 30343895; PubMed Central PMCID: PMCPMC6239978.

645 34. LaCourse KD, Peterson SB, Kulasekara HD, Radey MC, Kim J, Mougous JD. Conditional
646 toxicity and synergy drive diversity among antibacterial effectors. Nat Microbiol.
647 2018;3(4):440-6. Epub 2018/02/21. doi: 10.1038/s41564-018-0113-y. PubMed PMID:
648 29459733; PubMed Central PMCID: PMCPMC5876133.

649 35. Edgar RC. MUSCLE: multiple sequence alignment with high accuracy and high
650 throughput. Nucleic Acids Res. 2004;32(5):1792-7. doi: 10.1093/nar/gkh340. PubMed PMID:
651 15034147; PubMed Central PMCID: PMC390337.

652 36. Mistry J, Chuguransky S, Williams L, Qureshi M, Salazar GA, Sonnhammer ELL, et al.
653 Pfam: The protein families database in 2021. Nucleic Acids Res. 2021;49(D1):D412-D9. doi:
654 10.1093/nar/gkaa913. PubMed PMID: 33125078; PubMed Central PMCID:
655 PMCPMC7779014.

656 37. Waterhouse A, Bertoni M, Bienert S, Studer G, Tauriello G, Gumienny R, et al. SWISS-
657 MODEL: homology modelling of protein structures and complexes. Nucleic Acids Res.
658 2018;46(W1):W296-W303. doi: 10.1093/nar/gky427. PubMed PMID: 29788355; PubMed
659 Central PMCID: PMCPMC6030848.

660 38. Greener JG, Kandathil SM, Jones DT. Deep learning extends de novo protein
661 modelling coverage of genomes using iteratively predicted structural constraints. Nat
662 Commun. 2019;10(1):3977. Epub 20190904. doi: 10.1038/s41467-019-11994-0. PubMed
663 PMID: 31484923; PubMed Central PMCID: PMCPMC6726615.

664 39. Buchan DWA, Jones DT. The PSIPRED Protein Analysis Workbench: 20 years on.
665 Nucleic Acids Res. 2019;47(W1):W402-W7. doi: 10.1093/nar/gkz297. PubMed PMID:
666 31251384; PubMed Central PMCID: PMCPMC6602445.

667 40. Lai EM, Kado CI. Processed VirB2 is the major subunit of the promiscuous pilus of
668 Agrobacterium tumefaciens. J Bacteriol. 1998;180(10):2711-7. Epub 1998/06/06. PubMed
669 PMID: 9573157; PubMed Central PMCID: PMC107224.

670 41. Schindelin J, Arganda-Carreras I, Frise E, Kaynig V, Longair M, Pietzsch T, et al. Fiji: an
671 open-source platform for biological-image analysis. Nat Methods. 2012;9(7):676-82. Epub
672 20120628. doi: 10.1038/nmeth.2019. PubMed PMID: 22743772; PubMed Central PMCID:
673 PMCPMC3855844.

674 **FIGURE LEGENDS**

675 **Figure 1. V2c is a PAAR-linked specialized effector containing C-terminal Tox-**
676 **SHH motif. (A)** Schematic diagram of V2c protein showing N-terminal DUF4150
677 PAAR region and the catalytic region (amino acid 380-409) which covers the Tox-
678 SHH motif. **(B)** Partial sequence alignment of orthologs of V2c from BLASTP. The
679 strain name and accession number are indicated on the left. SHH motif is highlighted
680 in yellow, with H383 (indicated in red) as the metal ion coordinating residue, H384
681 and H408 (indicated in green) of HNH motif for catalysis and metal ion binding
682 respectively, are targeted for mutagenesis. The star corresponds to the specific
683 domains shown in Figure 1C: *DUF4150/PAAR-like, **DUF4150/PAAR-like + FIX-
684 like, ***FIX-like superfamily, **** PAAR + Rhs core domain. **(C)** Domain architectures
685 of V2c orthologs, Tox-SHH-containing proteins found in this study. Full length
686 sequences were analyzed and the domains were from Pfam database with E value

687 threshold set at 10^{-5}. **(D)** Cartoon model of V2c (residue 380-409). The structure of
688 V2c predicted by AlphaFold indicates V2c consisting a His-Me finger domain with
689 two antiparallel β-strands (yellow) connected with an Ω loop (light blue), a histidine
690 (H384) at the C-terminus of the first β-strand and followed by an α-helix (magenta).
691 The confidence score of this region is higher than 90, indicating high structure
692 accuracy.
693
694 **Figure 2. V2c exhibits growth inhibition, DNase activity *in vivo* and *in vitro.* (A)**
695 Growth inhibition analysis of expression of *v2c,* its variants, with or without *v3c* in *E.*
696 *coli* DH10B. *E. coli* cultures were induced with 1 mM IPTG at 0 hour for *v3c* expressed
697 from pTrc200 plasmid followed by L-arabinose (Ara) induction at 1 hour to induce *v2c*
698 from pJN105 plasmid. Cell growth was recorded every hour at OD_{600}. Strain
699 expressing empty vectors (vectors) were used as a control. **(B)** Number of colony
700 forming unit (log_{10} CFU/mL) quantified after growth inhibition assay at 8 hour. Data of
701 (A) and (B) represents mean ± SEM of four independent experiments (n=4), each
702 averaged with 3 technical repeats. Different letters above the bar indicate statistically
703 different groups of strains ($P < 0.05$) determined by Tukey's HSD test. **(C)** Plasmid
704 degradation assay performed by *E. coli* DH10B cells harboring pTrc200 and pJN105
705 plasmids (vector) or the derivatives induced with (+) or without (–) Ara for 2 hour.
706 Plasmid DNA was extracted and the degradation pattern was observed in agarose gel.
707 **(D)** *In vitro* DNase activity assay performed by using pTrc200HA plasmid DNA as DNA
708 substrate and incubated with purified V2c or its variants. Nuclease free water (ddH_2O),
709 protein elution buffer (elution buffer) and eluate from empty vector expression (pET28a)
710 served as negative controls while Benzonase nuclease served as a positive control.
711 The digestion of DNA substrate was determined by agarose gel electrophoresis. The
712 reaction samples of V2c or its variants were detected by western blotting using anti-
713 V2c antibody (α-V2c). Results of (C) and (D) are representative of three independent
714 experiments.
715
716 **Figure 3. V2c Tox-SHH DNase exhibits cell elongation phenotype. (A)** Images of
717 *E. coli* DH10B cells harboring vector(s) and the derivatives expressing *v2c* or its
718 variants in the presence or absence of its cognate immunity gene *v3c* with (+Ara) and
719 without (-Ara) Arabinose induction stained with FM-4-64 (red) and Hoechst stain (blue).
720 The micrographs from left to right are FM-4-64, Hoechst, phase contrast and a merged

721 image of FM-4-64 and Hoechst stains. Scale bar, 2 μm. Representative images of two
722 independent experiments are shown. **(B)** Normalized Hoechst intensity (intensity/unit
723 area of cells) and **(C)** Cell length (μm) as measured from the indicated number of cells
724 (n) per treatment. The graph shows a combined count from three frames of a
725 representative result of two independent experiments. The red line in (C) shows the
726 median with interquartile range. Statistics were performed with data mean ± SEM of
727 three frames. Different letters above the bar indicate statistically different groups of
728 strains ($P < 0.05$) determined by Tukey's HSD test.
729
730 **Figure 4. V2a Tox-AHH DNase exhibits cell elongation phenotype. (A)** Cartoon
731 model of V2a (residue 380-470). The structure of V2a predicted by AlphaFold indicates
732 V2a consisting of a His-Me finger domain with its signature antiparallel β-strands
733 (yellow) connected with an Ω loop (light blue) with a histidine (H386, orange) at the C-
734 terminus of the first β-strand. Two α-helices (pink) with histidine residues (H430, H456
735 magenta) followed the β-strands. N412 is found in the loop between the β-strands and
736 H430 is in the first α-helix (E429–G430). The predicted Local-Distance Difference Test
737 (pLDDTs) of the His-Me domains of V2a are from confident to very high, most of the
738 pLDDTs of the residues are > 90. **(B)** Morphological analysis of *E. coli* DH10B cells
739 harboring vector(s) or its derivatives expressing *v2a*, catalytic site (H385A) mutant
740 without (-Ara) or with (+Ara) arabinose induction. Cells were stained with FM-4-64 (red)
741 and Hoechst stain (blue). The micrographs from left to right are FM-4-64, Hoechst,
742 phase contrast and a merged image of the two fluorescent images. Scale bar, 2 μm.
743 **(C)** Cell length (μm) and **(D)** Hoechst intensity in different treatments as determined
744 from a combined count of three random frames of a representative result, the number
745 of cells (n) per sample is indicated. The graph shows a combined count from three
746 frames of a representative result of two independent experiments. The red line shows
747 the median with interquartile range. Statistics were performed with data mean ± SEM
748 of three frames. Different letters above the bar indicate statistically different groups of
749 strains ($P < 0.05$) determined by Tukey's HSD test.
750
751 **Figure 5. V2a and V2c exhibit different toxicity against *A. tumefaciens* and *D.***
752 ***dadantii*. (A)** Intra-species competition between *A. tumefaciens* 1D1609 attacker and
753 prey C58. **(B), (C), (D)** Inter-species competition between *A. tumefaciens* 1D1609
754 attacker and prey *D. dadantii* 3937 Δ*imp.* The plasmid pRL-GFP(S65T) plasmid (Gm^R)

755 was transformed into prey cells, which were mixed at 1:10 ratio with each of the
756 attacker strains, 1D1609 WT or various EI mutant strains as indicated. After co-culture
757 on AK agar plates, cells was collected, serially diluted, and plated on LB agar plate
758 containing Gm for CFU counting of surviving prey cells **(B)**. Data are mean ± SEM (n
759 = 6 biological repeats from three independent experiments). For imaging, co-cultured
760 *D. dadantii* Δ*imp*-GFP(S65T) and 1D1609 EI pair mutant were concentrated and
761 spotted on 2% agarose pad for fluorescence micrographs **(C)**. *D. dadantii* Δ*imp*-
762 GFP(S65T) indicated as Dd only is included as a control. The inset in phase contrast
763 shows a magnified image of cells in the red box. White arrows point to *D. dadantii* cells.
764 Scale bar, 2 μm. **(D)** Cell length after competition between *A. tumefaciens* 1D1609 EI
765 mutants with *D. dadantii* 3937 Δ*imp*-GFP(S65T). Cell length of GFP fluorescent *D.*
766 *dadantii* cells was measured using Fiji analyze particles tool. Cell length (μm) in
767 different treatments as determined from a combined count of at least 10 random
768 frames of two independent experiments. The red line shows the median with
769 interquartile range. Statistics were performed with data mean ± SEM of total counts.
770 Different letters above the bar indicate statistically different groups of strains ($P < 0.05$)
771 determined by Tukey's HSD test.
772
773 **Figure S1. Genetic loci of *A. tumefaciens* 1D1609 T6SS gene cluster and *vgrG***
774 **genetic modules.** The four *vgrG* genes (*vgrGa, vgrGb, vgrGc, vgrGd*) and their
775 associated effector-immunity pairs are indicated on linear chromosome. The number
776 of *vgrG*-associated genes *(v)* represents the position to *vgrG* as defined previously
777 [11].
778
779 **Figure S2. Sequence alignment of V2a and V2c.** The conserved amino acid
780 residues are indicated as '∗' (identical), ':' (similar) and '.' (slightly similar). The
781 DUF4150, PAAR-like domain is in green. The histidine residues in AHH and SHH
782 motifs in His-Me finger domain of V2a and V2c respectively, V2aH385/V2cH383 and
783 V2aH386/V2cH384, are in red. The histidine residues that predicted to responsible for
784 metal binding in His-Me finger domain, V2aH430/V2cH408, are in a bold blue font.
785 Two peptides used for generating antibodies were underlined.
786

787 **Figure S3. Cell length analysis of *E. coli* DH10B cells expressing *v2c* catalytic**
788 **site variants. (A)** Expression of *v2c* single catalytic site variants. **(B)** Expression of
789 catalytic site variants co-expressed with *v3c*. Cell length (μm) as measured from the
790 indicated number of cells (n) per sample. The graph shows a combined count from six
791 random frames of a representative result, the number of cells (n) per sample is
792 indicated. The graph shows a combined count from 6 random frames, 3 from each of
793 two independent experiments. The red line shows the median with interquartile range.
794 Statistics were performed with data mean ± SEM of 6 frames. Different letters above
795 the bar indicate statistically different group of strains ($P < 0.05$) determined by Tukey's
796 HSD test. The red line shows the median with interquartile range.
797
798 **Figure S4. V4b exhibits growth inhibition, which could be neutralized by V5b.**
799 **(A)** Schematic diagram of V4b. The Rhs domain is bordered by conserved motifs. The
800 CT is the C-terminal domain encoding a putative muramidase toxin. **(B)** *E. coli* growth
801 inhibition analysis. *E. coli* DH10B cultures were induced with 1 mM IPTG at 0 hour for
802 the expression of putative immunity gene *v5b* from pTrc200 plasmid followed by L-
803 arabinose (Ara) induction at 1 hour to induce putative *v4b* toxin gene from pJN105
804 plasmid. Cell growth was recorded every hour at OD_{600}. DH10B expressing empty
805 vectors were used as a control. Data are mean ± SD of three biological replicates.
806 Similar results were observed in three independent experiments. **(C)** Plasmid
807 degradation assay performed by using full length V4b ($v4b^{FL}$) and C-terminal domain
808 only ($v4b^{CT}$). *E. coli* cells with pTrc200 and pJN105 plasmid (vectors) or expressing
809 *v4b* and *v4b*+*v5b* were induced with (+) or without (-) arabinose (Ara) for 2 h. Plasmid
810 DNA was extracted and the degradation pattern was observed in agarose gel. Result
811 shown is a representative data from two independent experiments. **(D)** Images of *E.*
812 *coli* DH10B cells expressing *v4b* and *v4b* co-expressed with its cognate immunity gene
813 *v5b* (*v4b*+*v5b*) under condition with (+Ara) or without (-Ara) arabinose induction. *E.*
814 *coli* DH10B cells expressing empty vectors (vectors) under condition with (+Ara) and
815 without (-Ara) arabinose induction served as negative controls. Cells were stained with
816 FM-4-64 (red) and Hoechst stain (blue). The micrographs from left to right are FM-4-
817 64, Hoechst, phase contrast and a merged image of the two fluorescent micrographs.
818 Representative images of two independent experiments are shown. Scale bar, 2 μm.
819 **(E)** Cell length (μm) and **(F)** Hoechst intensity in cells analyzed in (D). The red line
820 shows the median with interquartile range. The graph shows a combined count from

821 3 random frames of a representative result, the number of cells (n) per sample is
822 indicated Statistics were performed with data mean ± SEM of three frames. Different
823 letters above the bar indicate statistically different groups of strains ($P < 0.05$)
824 determined by Tukey's HSD test.
825
826 **Supplementary Table S1.** Bacterial strain and plasmids used in this study
827
828 **Supplementary Table S2.** Primers used in this study**.**
829

Figure 1. V2c is a PAAR-linked specialized effector containing C-terminal Tox-SHH motif.

(A)

(B)

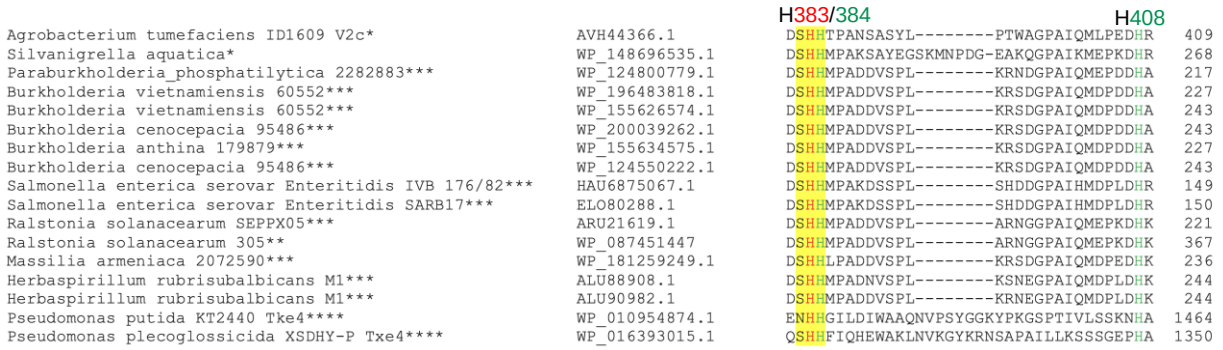

		H383/384 H408	
Agrobacterium tumefaciens ID1609 V2c*	AVH44366.1	DSHHTPANSASYL--------PTWAGPAIQMLPEDHR	409
Silvanigrella aquatica*	WP_148696535.1	DSHHMPAKSAYEGSKMNPDG-EAKQGPAIKMEPKDHR	268
Paraburkholderia_phosphatilytica 2282883***	WP_124800779.1	DSHHMPADDVSPL--------KRNDGPAIQMEPDDHA	217
Burkholderia vietnamiensis 60552***	WP_196483818.1	DSHHMPADDVSPL--------KRSDGPAIQMDPDDHA	227
Burkholderia vietnamiensis 60552***	WP_155626574.1	DSHHMPADDVSPL--------KRSDGPAIQMDPDDHA	243
Burkholderia cenocepacia 95486***	WP_200039262.1	DSHHMPADDVSPL--------KRSDGPAIQMDPDDHA	243
Burkholderia anthina 179879***	WP_155634575.1	DSHHMPADDVSPL--------KRSDGPAIQMDPDDHA	227
Burkholderia cenocepacia 95486***	WP_124550222.1	DSHHMPADDVSPL--------KRSDGPAIQMDPDDHA	243
Salmonella enterica serovar Enteritidis IVB 176/82***	HAU6875067.1	DSHHMPAKDSSPL--------SHDDGPAIHMDPLDHR	149
Salmonella enterica serovar Enteritidis SARB17***	ELO80288.1	DSHHMPAKDSSPL--------SHDDGPAIHMDPLDHR	150
Ralstonia solanacearum SEPPX05***	ARU21619.1	DSHHMPADDVSPL--------ARNGGPAIQMEPKDHK	221
Ralstonia solanacearum 305**	WP_087451447	DSHHMPADDVSPL--------ARNGGPAIQMEPKDHK	367
Massilia armeniaca 2072590***	WP_181259249.1	DSHHLPADDVSPL--------KRSDGPAIQMDPEDHK	236
Herbaspirillum rubrisubalbicans M1***	ALU88908.1	DSHHMPADNVSPL--------KSNEGPAIQMDPLDHK	244
Herbaspirillum rubrisubalbicans M1***	ALU90982.1	DSHHMPADDVSPL--------KRNEGPAIQMDPLDHK	244
Pseudomonas putida KT2440 Tke4****	WP_010954874.1	ENHHGILDIWAAQNVPSYGGKYPKGSPTIVLSSKNHA	1464
Pseudomonas plecoglossicida XSDHY-P Txe4****	WP_016393015.1	QSHHFIQHEWAKLNVKGYKRNSAPAILLKSSSGEPHA	1350

(C)

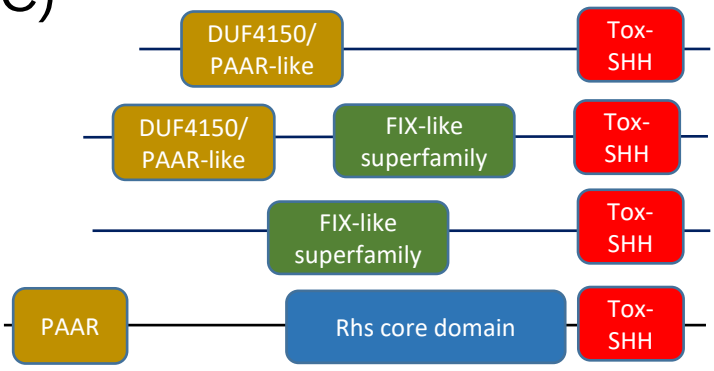

(D)

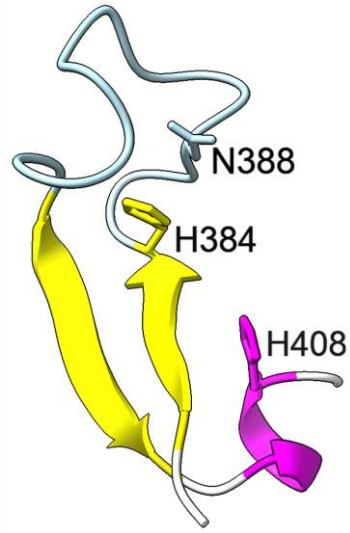

Figure 2. V2c exhibits growth inhibition, DNase activity *in vivo* and *in vitro*.

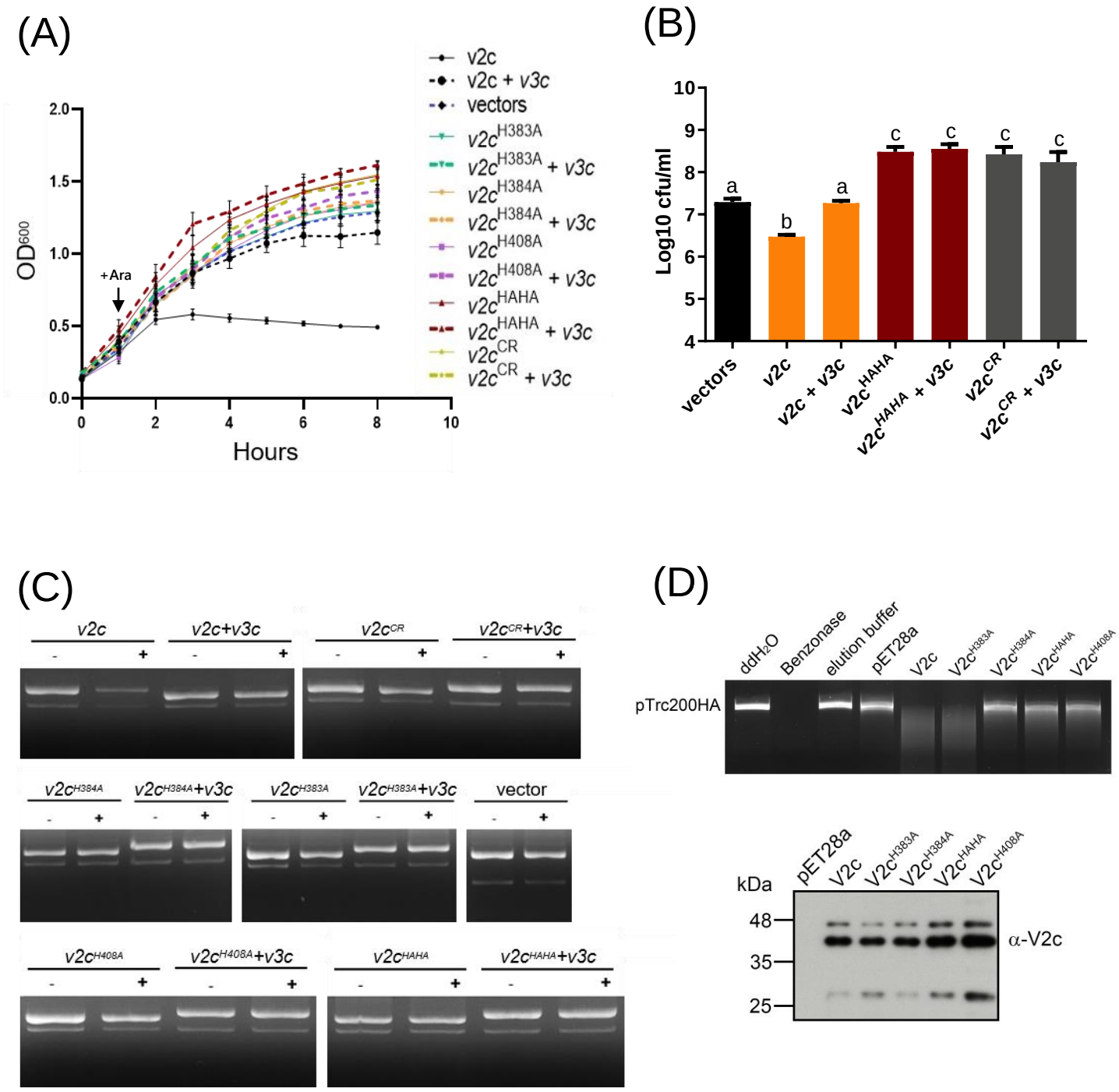

Figure 3. V2c Tox-SHH DNase exhibits cell elongation phenotype.

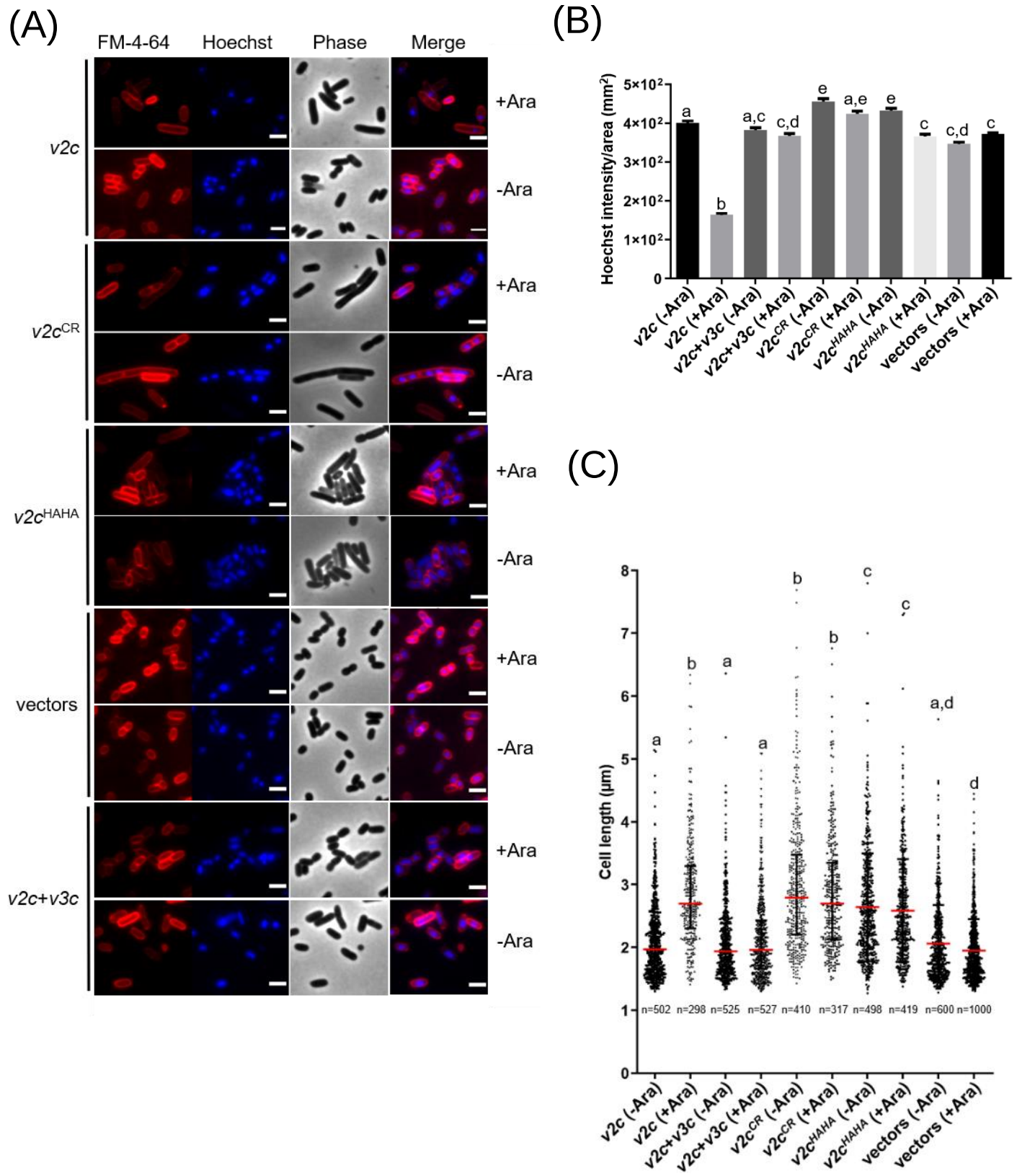

Figure 4. V2a Tox-AHH DNase exhibits cell elongation phenotype.

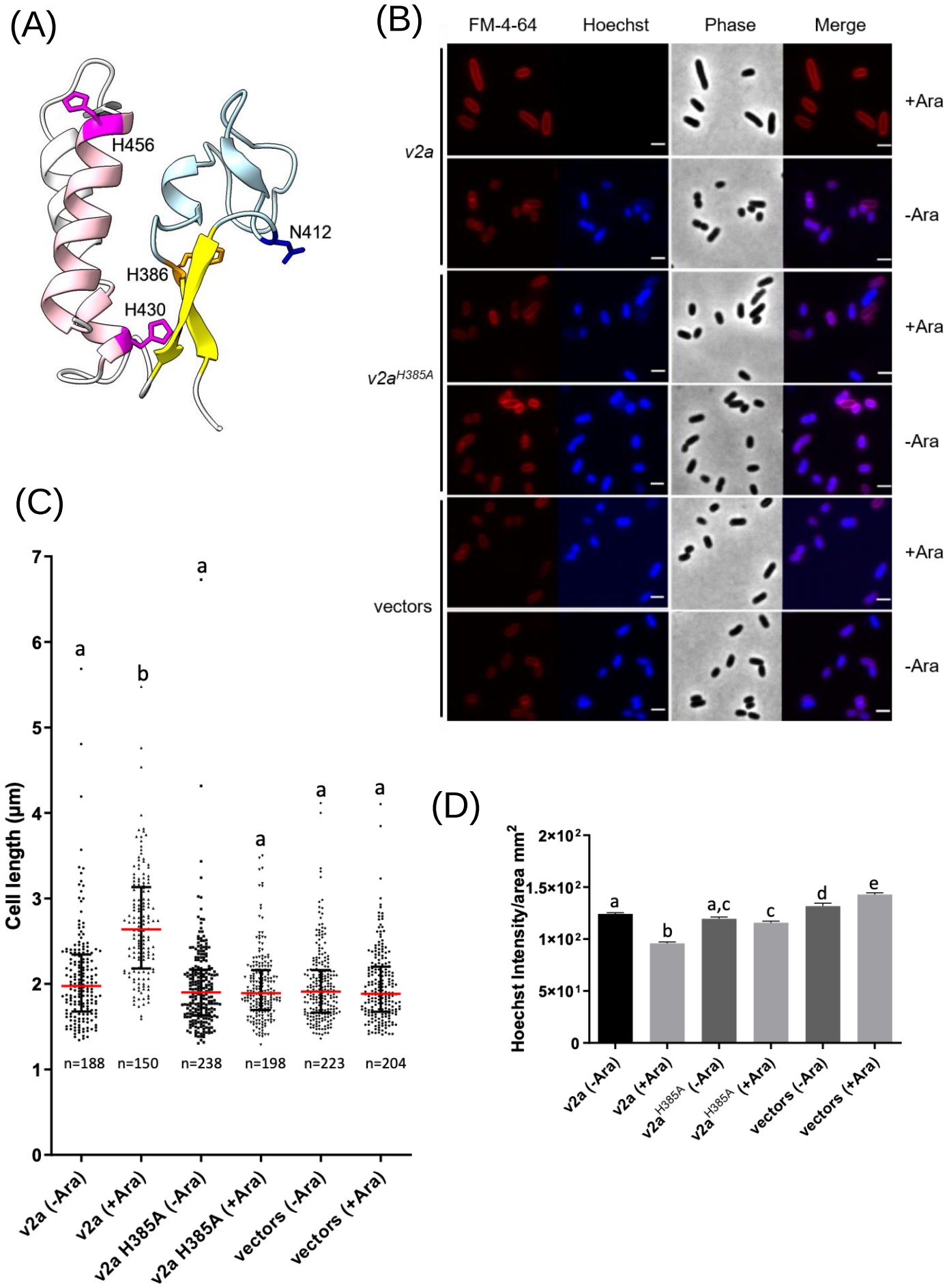

Figure 5. V2a and V2c exhibit different toxicity against *A. tumefaciens* and *D. dadantii*.

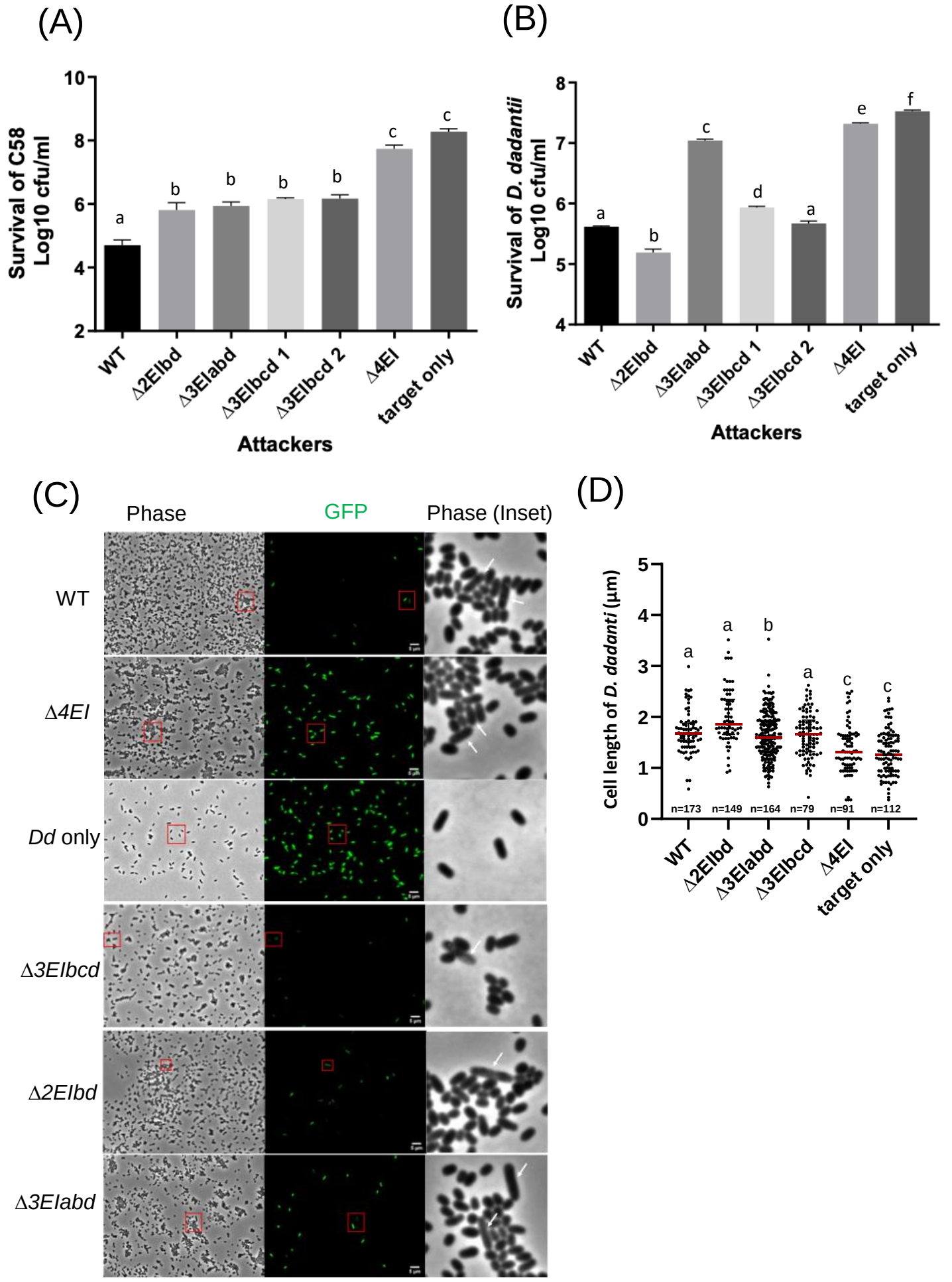

Figure S1. Genetic loci of *A. tumefaciens* 1D1609 T6SS gene cluster and *vgrG* genetic modules.

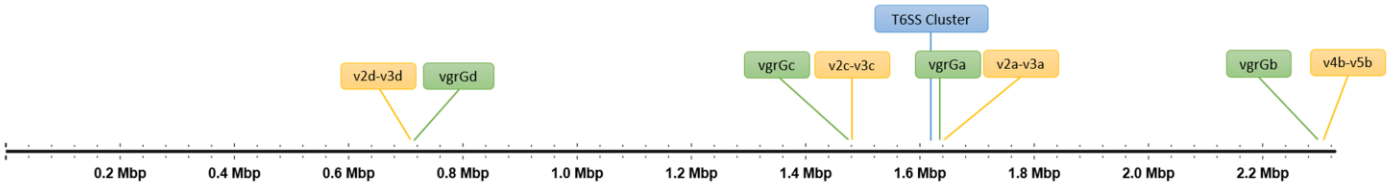

Figure S2. Sequence alignment of V2a and V2c.

```
V2a             MSIPRDNYIGEPQYPGTWTTATPREGLRDIDEARIVSLAPDVCLTPVGSSVVPIPYPVVD
V2c             MSIPRDNYIGEPQYPGTWTTATPREGLRDIDEARIVSLAPDVCLTPVGSSVVPIPYPVVD
                ************************************************************
V2a             FCGHDKNYTPSVRFTGKKAMVMRSFTTHVHGDAPGNRKGVKSGTVESICEPIGHADQVRA
V2c             FCGHDKNYTPSVRFTGKKAMVMRSFTTHVHGDAPGNRKGVKSGTVESICEPIGHADQVRA
                ************************************************************
V2a             EGSHVIRHLDRFYMNSRNTQGEAIFVRSTQTYDPPKDDDPVRGSLRWQDGSDEGRVMSDA
V2c             EGSHVIRHLDRFYMNSRNTQGEAIFVRSTQTYDPPKDDDPVRGSLRWQDGSDEGRVMSDA
                ************************************************************
V2a             SPEPFKEGEKYAYAGSAAAATTGAAQNSAQALRGGMPATRPTVPQTVPRGPGRVITPGPA
V2c             SPEPLIMGAQYAQAQTATIPQSGGV-----ARRGTYGRPTTTVDPRLLKGL-RFWSSARG
                ****:  * :** * :*: . :*..     * **    . .**   : .*  *. :.. .
V2a             RAP---QWYRTPPHRVVSDLA-KVG---------RLARVGIWAR-RLNVIGILSSVLIPD
V2c             AAEIMDMVQQISEDRAVQDSAGQLGLNLSDPTDVLVARAHAWSKYHIDASPFYWD--FPN
                 *       . .  *.*.* * ::*          :**.  *:. .::.  :  .  :*:
V2a             NGANLSDVVPRDDQERRIKEMFDEGVDAGHDSWEMRDWAMEELRRHRQRVREEPESRPQA
V2c             SQ------VGRDAATKAITSM--EAAAPG----TLGE-ALQGDRTQLEKLRTAIKNAVSA
                .       * **   . *..*  *.. .*     : : *::  * : :.:*   :.  .*
V2a             LPQSETVRVSDRDEYRKKCQVDRYGKMKSVCGQYGMQAHHIVPDWTLRYGAREEADKRIP
V2c             ATAAASVRVSG-----QPCAREALG----APGKYRGGAHFAT---ALPLGDNLDSHHTPA
                 . : :****.     : *  :  *    . *:*   **. .   :*  * . :: :  .
V2a             NMPSLNDGMAICVIGNARVEQTEHWGGHLAD------KAIENAGRNSTPPFTAPLHKVVQ
V2c             NSASY----------------LPTWAGPAIQMLPEDHRATLSYGRKVTSPYISTQARLIN
                * .*                    *.*   :      .*  . **: *.*: :.  .:::
V2a             ASAQAMISVRPDCAKEIMAALTTQYAGKNPFQLLRAK--QYPPLPEETISALKSGAVEGA
V2c             SG-------------QFMKAINMDILDIKRIAMLRGDPTRYDAAIAQMMAYAECLKREGI
                :.             ::* *:. :  . : : :**..  .* .   : ::  :.   **
V2a             TRKP
V2c             IK--
                 .
```

Figure S3. Cell length analysis of *E. coli* DH10B cells expressing *v2c* catalytic site variants.

(A)

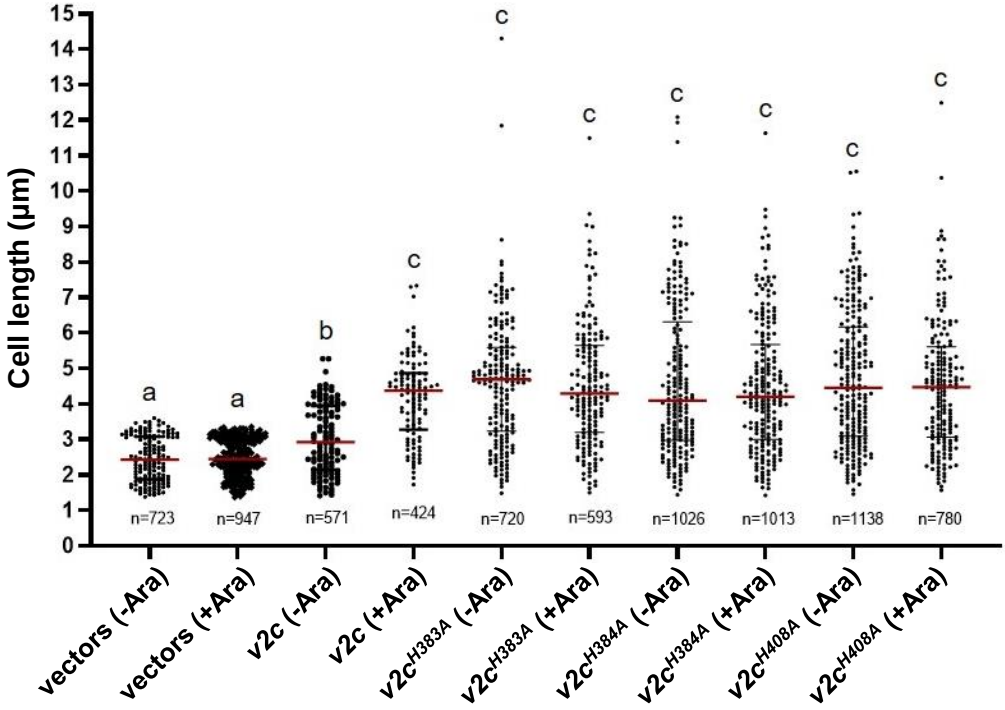

(B)

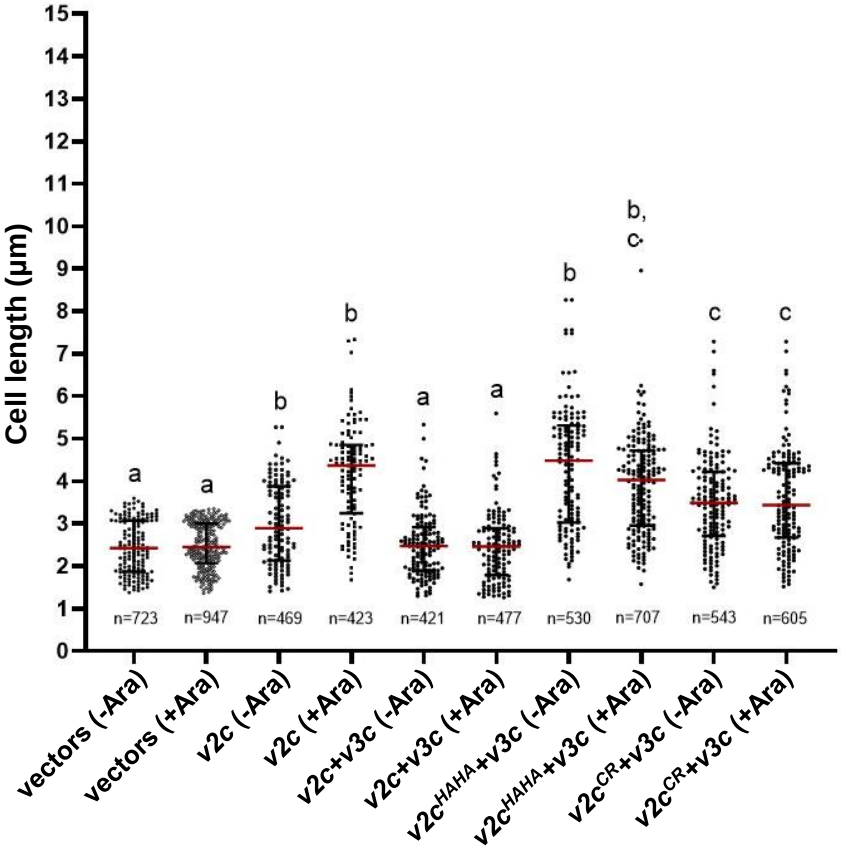

Figure S4. V4b exhibits growth inhibition, which could be neutralized by V5b.

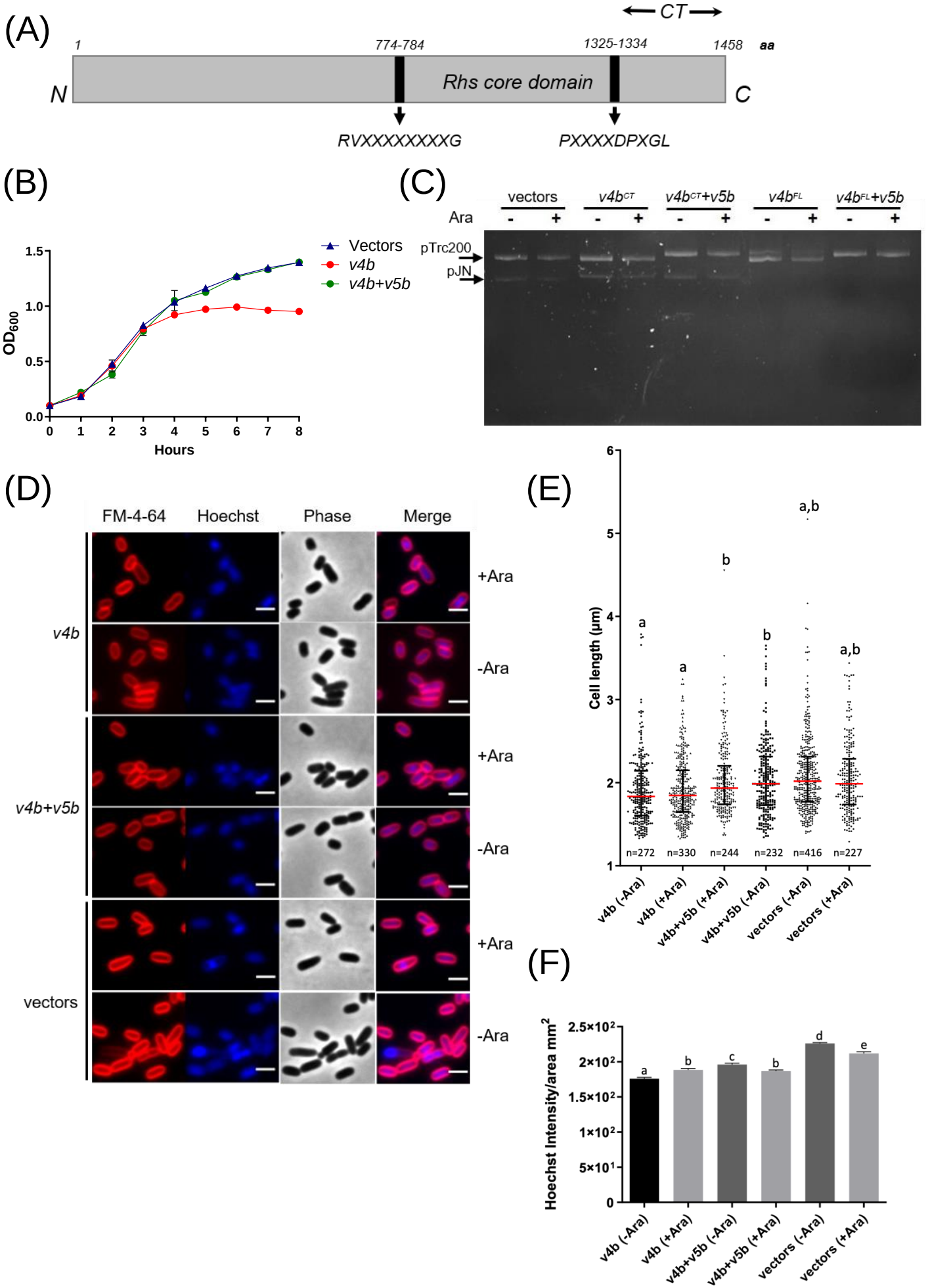

Table S1. Bacterial strains and plasmids

Strain	Relevant characteristics	Reference/Source	EML No.
E. coli			
DH10B	Host of plasmid for cloning	Lab stock	EML455
S17-1	Host for conjugation	Lab stock	EML124
BL21 (DE3)	For protein expression	Lab stock	EML117
***D. dadantii* 3937**			
WT	Wild-type *Dickeya dadantii* 3937	Ching-Hong Yang, University of Wisconsin, Milwaukee	EML4911
Δ*imp*	T6SS inactive strain with deletion of *imp* operon	Ching-Hong Yang, University of Wisconsin, Milwaukee	EML4921
***A. tumefaciens* 1D1609**			
WT	Alfalfa isolate, virulent strain containing pTi1D1609	Clarence Kado, UC Davis	EML304
Δ*4* or Δ*vgrGabcd*	Deletion of *vgrGa*, *vgrGb*, *vgrGc* and *vgrGd*	Santos et al., 2020	EML4746
Δ2*EIbd*	Deletion of *vgrGb*- and *vgrGd*-associated effector-immunity pair	This study	EML5531
Δ3EIbcd #1	Deletion of *vgrGb*-, *vgrGc*- and *vgrGd*-associated effector - immunity pair using Δ2EIbc as background.	This study	EML5594

Δ3EIbcd #2	Deletion of *vgrGb*-, *vgrGc*- and *vgrGd*-associated effector - immunity pair using Δ2EIcd as background.	This study	EML5920
Δ3*EIabd*	Deletion of *vgrGa*-, *vgrGb*- and *vgrGd*-associated effector - immunity pair	Santos et al., 2020	EML5515
Δ4*EIabcd*	Deletion of *vgrGa*-, *vgrGb*- and *vgrGd*-associated effector - immunity pair and whole *vgrGc* cluster (Δ*vgrGc-v3*)	Santos et al., 2020	EML5540
Plasmids			
pJQ200KS	Gm^R, suicide plasmid containing GmR and sacB gene for selection of double crossover	Quandt and Hynes, 1993	EML121
pRL662	Gm^R, broad host range vector derived from pBBR1MCS-2	Vergunst et al., 2000	EML315
pTrc200	Sp^R, pVS1 origin, *lacIq, trc* promoter expression vector	Schmidt-Eisenlohr et al., 1999	EML904
pJN105	Gm^R, arabinose-inducible gene expression vector derived from pBBRMCS-1, *araC*-P_{BAD}	Newman and Fuqua, 1999	EML4220
pET28a	Km^R, Protein expression vector, N-terminal His-tagged	Lab stock	EML2485

pJN-*v2a*	Gm^R, pJN expressing *v2a*	Santos et al., 2020	EML5272
pJN-*v4b*^{FL}	Gm^R, pJN expressing the full-length *v4b*	This study	EML4758
pJN-*v4b*^{CT}	Gm^R, pJN expressing the C-terminal toxin domain of *v4b*	This study	EML4756
pJN-*v2c*	Gm^R, pJN expressing *v2c*	This study	EML5328
pTrc-*v5b*	Sp^R, pTrc200 expressing the immunity protein V5b	This study	EML4759
pTrc-*v3c*	Sp^R, pTrc200 expressing the immunity protein V3c	This study	EML5337
pJN-*v2a* (H385A)	Gm^R, pJN expressing *v2a* with amino acid substitution (H385A)	Santos et al., 2020	EML5298
pJN-*v2c* (H383A)	Gm^R, pJN expressing *v2c* with amino acid substitution (H383A)	This study	EML5925
pJN-*v2c* (H384A)	Gm^R, pJN expressing *v2c* with amino acid substitution (H384A)	This study	EML5926
pJN-*v2c* (H408A)	Gm^R, pJN expressing *v2c* with amino acid substitution (H408A)	This study	EML5927
pJN-*v2c* (HAHA)	Gm^R, pJN expressing *v2c* with amino acid substitution (H383AH384A)	This study	EML5922
pJN-*v2c* CR	Gm^R, pJN expressing *v2c* with deletion of the conserve region of Tox-SSH domain	This study	EML5589
pJQ200sk-*vag4vag5b*	Gm^R, plasmid to generate Δ3*EIbcd* #2	This study	EML5307

pJQ200sk-*vag2vag3d*	Gm^R, plasmid to generate Δ2*EIbd*, Δ3*EIbcd* #1 and Δ3*EIabd*	This study	EML5340
pRL662-GFP(S65T)	GFP from pRU1156 cloned into pRL662	Lab stock	EML3376
pET28a-*v2c*	pET28a expressing His-tagged V2c	This study	EML6050
pET28a-*v2c*HAHA	pET28a expressing His-tagged V2c H383AH384A	This study	EML6051
pET28a-*v2c*H408A	pET28a expressing His-tagged V2cH408A	This study	EML 6063
pET28a-*v2c*H383A	pET28a expressing His-tagged V2cH383A	This study	EML 6064
pET28a-*v2c*H384A	pET28a expressing His-tagged V2cH384A	This study	EML 6065

Table S2. Primers used in this study

Primer Name	Sequences	Purpose
V2c(H383A)	5'-CCGGAATTCAAGGAACAGCTATGAGCATCCCCCGCGAC-3' 5'- GACAATTTAGATAGCGCGCATACTCCTGCTAACTCT-3' 5'- AGAGTTAGCAGGAGTATGCGCGCTATCTAAATTGTC-3' 5'- CGTCTAGATCACTTTATGATTCCTTCGCG-3'	mutagenesis
V2c(H384A)	5'-CCGGAATTCAAGGAACAGCTATGAGCATCCCCCGCGAC-3' 5'-GACAATTTAGATAGCCATGCGACTCCTGCTAACTCT-3' 5'-AGAGTTAGCAGGAGTCGCATGGCTATCTAAATTGTC-3' 5'- CGTCTAGATCACTTTATGATTCCTTCGCG-3'	mutagenesis
V2c(H408A)	5'-CCGGAATTCAAGGAACAGCTATGAGCATCCCCCGCGAC-3' 5'- ATGCTTCCAGAAGACGCGCGAGCTACACTCTCATAT -3' 5'-TGAGAGTGTAGCTCGCGCGTCTTCTGGAAGCAT-3' 5'- CGTCTAGATCACTTTATGATTCCTTCGCG-3'	mutagenesis
V2c(CR)	5'-GTTTTTTTGGGCTAGCGAAGGAACAGCTATGAGCATC-3' 5'-CCTTTCTTCCATATGAGAGTGTAGCATTGTCGCCAAGTGGGAGGGCCGTC-3' 5'-GACGGCCCTCCCACTTGGCGACAATGCTACACTCTCATATGGAAGAAAGG -3' 5'-GCGGTGGCGGCCGCTTCACTTTATGATTCCTTCGC-3'	mutagenesis
V2c(H383A H384A)	5'-CCGGAATTCAAGGAACAGCTATGAGCATCCCCCGCGAC-3' 5'-GACAATTTAGATAGCCATGCGACTCCTGCTAACTCT-3' 5'-AGAGTTAGCAGGAGTCGCATGGCTATCTAAATTGTC-3' 5'- CGTCTAGATCACTTTATGATTCCTTCGCG-3'	mutagenesis
pJQ200KS-*v4bv5b*	5'-TTTCTAGACATCTGTTGTTCGCGGCCGATG-3' 5'-GCGGATCCATCACCCGCCATGTGAGGCCT-3' 5'-GCGGATCCTTCGCTGCCCTGTGACCGTTCT-3' 5'-GCCCCGGGGCAAGATGATTCCGGGAATTGAC-3'	deletion mutant
pJQ200KS-v2dv3d	5'-GCTCTAGAGAGCGCCGAAATCCGCTT-3' 5'-CGGGATCCGATGCTCATGCTGTCTCCCTCTC-3' 5'-CGGGATCCGCCAGAAAGCCATAGATTGTCG-3' 5'-TCCCCCCGGGGCATCACCACACTCTCGAGCCT-3'	deletion mutant

V4b	5'-CCGTCTAGAAAGGAACAGCTATGGCGGGTGAT-3' 5'-CGGAGCTCGTTTCGATACTCAGCATCGACCG-3'	overexpression
V5b	5'-TATAGGTACCCGAGAATAAGAACCGCGTTC-3' 5'-GCTCTAGAATTGGCGAGGCTACAGCG-3'	overexpression
V2c	5'-CCGGAATTCAAGGAACAGCTATGAGCATCCCCCGCGACAATTAT-3' 5'-CGTCTAGATCACTTTATGATTCCTTCGCGTTTAAGGC-3'	overexpression
V3c	5'-ATCCGAGCTCGTGACAGACAAGTCGGGAGCG-3' 5'-GCTCTAGACCTAGATCCATCGCTTACTGCCTC-3'	overexpression

pET28a-v2c	5'-AATCTAGAATGAGCATCCCCCGCGACAA-3'. 5'-AACTCGAGCTTTATGATTCCTTCGC-3'	Protein expression
pET28a-v2cHAHA	5'-GACAATTTAGATAGCGCGGCGACTCCTGCTAACTCT-3'. 5'-AGAGTTAGCAGGAGTCGCCGCGCTATCTAAATTGTC-3'	Protein expression
pET28a-v2c-H383A	5'-GACAATTTAGATAGCGCGCATACTCCTGCTAACTCT-3' 5'-AGAGTTAGCAGGAGTATGCGCGCTATCTAAATTGTC-3'	Protein expression
pET28a-v2c-H384A	5'-GACAATTTAGATAGCCATGCGACTCCTGCTAACTCT-3' 5'-AGAGTTAGCAGGAGTCGCATGGCTATCTAAATTGTC-3'	Protein expression
pET28a-v2c-H408A	5'-ATGCTTCCAGAAGACGCGCGAGCTACACTCTCATAT-3' 5'-TGAGAGTGTAGCTCGCGCGTCTTCTGGAAGCAT-3'	Protein expression

Restriction enzyme sites are underlined. UF (upstream forward), UR (upstream reverse), DF (downstream forward) and DR (downstream reverse).